NBSIR 76-1181

METALLURGICAL EVALUATION AND FRACTURE ANALYSIS OF A PNEUMATICALLY-BURST SEAMLESS STEEL COMPRESSED GAS CYLINDER

Bruce W. Christ and John H. Smith

Mechanical Properties Section
Metallurgy Division
Institute for Materials Research
National Bureau of Standards
Washington, D.C. 20234

Failure Analysis Report

April, 1977

Prepared for
Office of Hazardous Materials Operations
Department of Transportation
Washington, D.C. 20590

Contract No. DOT AS-40034

U.S. DEPARTMENT OF COMMERCE, Juanita M. Kreps, *Secretary*
Dr. Betsy Ancker-Johnson, *Assistant Secretary for Science and Technology*
NATIONAL BUREAU OF STANDARDS, Ernest Ambler, *Acting Director*

NOTICE

The contents of this report reflect the views of the authors who are responsible for the facts and the accuracy of the data presented herein. The contents do not necessarily reflect the official views or policy of the Department of Transportation. This report does not constitute a standard, specification or regulation.

This document is disseminated under the sponsorship of the Department of Transportation in the interest of information exchange. The United States Government assumes no liability for its contents or use thereof.

TABLE OF CONTENTS

TABLE OF CONTENTS (continued)

Metallurgical Evaluation and Fracture Analysis of a
Pneumatically-Burst Seamless Steel Compressed Gas Cylinder

1. GENERAL INFORMATION

1.1 Reference

U.S. Department of Transportation, Bureau of Hazardous Materials, Office of Hazardous Materials Operations, Engineering Branch, 2100-2nd Street, S.W., Washington, D.C. 20590. This report was prepared at the request of Mr. Arthur J. Mallen, Engineering Branch Chief, in a letter dated October 20, 1975.

1.2 Background

Sometime during July, 1975, a seamless steel gas cylinder in oxygen service exploded while it was being refilled. The event occurred near San Francisco, California. It was reported that the pneumatic burst occurred at a pressure of about 2500 psi. It was also reported that the bursting cylinder grazed the ankle of the operator on the filling platform, but that no substantial injury or other damage occurred.

The burst gas cylinder was crated and shipped to the National Bureau of Standards for examination, at the request of Mr. Arthur J. Mallen and with the concurrence of the operator of the gas cylinder filling facility. The crated cylinder arrived at NBS on or about September 12, 1975. Mr. Mallen also supplied a copy of the test report prepared by the disinterested inspector licensed by the Department of Transportation to carry out inspections and testing during gas cylinder manufacture.

Four preliminary reports on this cylinder were sent to the Office of Hazardous Materials Operations[1].

1.3 Identification and Description

The seamless steel gas cylinder is identified as follows:

Specification	DOT 3AA 2265
Test Date	12-74
Date of Test Report	January 8, 1975
Serial Number	T-0967
Identifying Symbol	PST
Type	H
Model	8BC250
Minimum Sidewall	0.207-inches
Heat Code	V18
Type of Steel	"Intermediate Manganese," quenched and tempered
Water Capacity	95.3 pounds, minimum
Size	8 9/16-inches inside diameter 51-inches length

Specification DOT 3AA can be found in section 178.37 of Title 49 of the Code of Federal Regulations[2].

A picture of the as-received cylinder appears in Figure 1a, where it is shown with an intact cylinder of the same size for comparison. The two halves of the neck appear at the upper left center and lower right center. An overall view including the bottom appears in Figure 1b. All the metal of the cylinder appeared to have remained together, despite the bursting forces. However, the neck ring and valve were not found in the shipment.

Identifying markings found on the cylinder appear in Figure 2. The Department of Transportation stamping at the neck end is in Figure 2a. The test date and other stamping appear in Figure 2b. The heat code, V18, was stamped on the bottom of the cylinder, Figure 3.

2. PURPOSE

The purpose of this report, as indicated in the request letter, is fourfold:

- to evaluate compliance of the cylinder with those requirements of Specification DOT 3AA which relate to chemistry, magnetic particle inspection, tensile properties and wall thickness.
- to carry out failure analysis.
- to carry out certain tests not appearing in Specification DOT 3AA.
- to carry out a stress analysis via fracture mechanics.

3. COMPARISON OF TEST RESULTS WITH REQUIREMENTS OF SPECIFICATION DOT 3AA

3.1 Chemical Analysis

Chemical analysis was carried out on a specimen cut from the bottom of cylinder T-0967. Results appear in Table I, along with a tabulation of the specification requirements. It is clear that these results comply with the chemistry requirements in section 178.37-5-(a) of specification DOT 3AA for "intermediate manganese" steel.

There is no requirement in specification DOT 3AA on the concentration of the residual elements cited in Table II. However, the concentrations of residual elements fall within the limits defined in the American Iron and Steel Institute Steel Products Manual[3], a widely recognized specification for the chemistry of steels.

Titanium is not included in either the DOT specification or the AISI specification. The rather high concentration of titanium, 0.03 weight percent, is notable, however. For this much titanium to be present, it

is likely that the titanium was added at some late stage in the steel making process to deoxidize the molten steel. Traditionally, silicon and aluminum serve as deoxidizing agents. The use of titanium as a deoxidizer of commercial heats of steel has been increasing in recent years.

Additions of deoxidants lead to the formation of oxide and nitride inclusions. Furthermore, sulfur combines with manganese to produce manganese sulfide inclusions. Analysis of the inclusions in this steel is reported in Section 5.2, where it is shown that manganese sulfide is the predominant type of inclusion, as is the case for most steels.

3.2 Magnetic Particle Inspection

Magnetic particle inspection was applied to the exterior and interior surfaces of the as-received cylinder. No cracks were detected. Since this inspection was applied to the burst cylinder, it is concluded that the as-manufactured cylinder must have conformed to the requirements of section 178.37-11-a-(6) of specification DOT 3AA[2].

3.3 Tensile Properties

Four longitudinal tensile specimens were prepared in accord with section 178.37-16-(b) of specification DOT 3AA[2]. Because the as-received cylinder was distorted as shown in Figure 1, material was flattened at room temperature in a press before machining the tensile specimens. This material was taken as close as possible to the origin of fracture. Test results appear in Table III. Cold work introduced during catastrophic failure or flattening would have the tendency to raise the strength of the material. Yield strength is usually more sensitive to cold work than is tensile strength.

In section 178.37-17-(a) of specification DOT 3AA, it is required that elongation in the tensile test be "...at least 20 percent for 2" gauge length...". Results in Table III show that this requirement was met by all four tensile specimens, and that the average elongation exceeded the minimum required by 8.2 percent. Furthermore, ductility data which appear in Table III compare favorably with results which appear in the test report.

A notable feature of the tensile strengths in Table III is that they are about 7% lower than the tensile strengths appearing in the test report. The reasons for this difference are not known.

3.4 Wall Thickness

Wall thickness measurements were made along the fracture surfaces of the burst gas cylinder. Results are shown in Table IV, where the sidewall thickness ranges from 0.220 to 0.260-inches. Using the minimum measured wall thickness, 0.220-inches, the wall stress at test pressure was

calculated from the formula in section 178.37-10-(c) of specification DOT 3AA,

$$S = \frac{P(1.3D^2 + 0.4d^2)}{D^2 - d^2} = 3775\ (1.3(9.003)^2 + 0.4\ (8.563)^2)/$$

$$((9.003)^2 - (8.563)^2) = 65{,}800 \text{ psi.}$$

This wall stress slightly exceeds the allowable wall stress at test pressure of 64,500 psi, which is determined by taking 67% of the minimum tensile strength of the steel, 96,800 psi, as defined in section 178.37-10-(b) of specification DOT 3AA. Hence, this requirement was not met. However, this wall stress does not exceed the value of 66,900 psi, which results from taking 67% of the average tensile strength reported in Table III.

4. FRACTURE DESCRIPTION

4.1 Origin of Fracture

The pneumatically-burst cylinder was split by three longitudinal tears running from top to bottom, as is evident in Figure 1. Shear fracture was the principal fracture mode. The six longitudinal fracture surfaces --- all of which were relatively unrusted in the as-received condition --- were scanned visually for evidence of fracture origins. Only one region was found which was suspected of being a fracture origin. The two sides of this region are labeled a and a' in Figure 1b --- the region is about 10-inches below the neck.

The side of the origin labeled a' in Figure 1b is shown at two different angles in Figures 4a and 4b. The origin consists of:

1. A rusty and discolored region about 3-inches long, with elliptical ends. This region penetrates about 91% of the wall thickness.

2. A narrow, unrusted highly-reflective band along the inside wall, spanning about 9% of the wall thickness.

3. A small step of perhaps 3/16-inch near the neck end.

4. A gouge beneath the step.

5. Some lips of raised metal on the external surface.

6. Some rusted regions where paint was missing.

Figure 5 shows the side of the fracture origin labeled a in Figure 1b. The step and highly-reflective band along the inside wall are evident. Dimensions of the fracture origin are shown in the schematic diagram included in Figure 5.

The fracture surface within the origin was fibrous, except on the step. In the as-received condition, the step showed up as a smooth and brightly-reflecting surface. The smoothness of the step contrasts with the fibrous nature of the adjacent fracture surface in Figure 6, which was obtained with the scanning electron microscope.

Mating halves of the origin were cut out and placed together as shown in Figure 7 to give an approximate picture of the configuration before burst. Curvature of the pieces --- which probably developed during burst --- prevented precise matching. The lips of raised metal on the side which appeared in Figure 4b are evident in Figure 7. Here, they

have the appearance of having been flattened somewhat. The other side of the fracture origin shows regions where it had apparently been gouged.

To examine the fracture origin more closely, metallographic sections were cut from one side of the origin only. The other side was preserved intact. Specimens II, III and IV, as labeled in Figure 7, were cut to show the fracture profile at the origin. Specimen I near the origin was cut to show the fracture profile in the region of the fast-running crack. A specimen including the step was cut for examination of the fracture origin in the scanning electron microscope.

Figure 8 shows the fracture profile at Specimen IV. A gouge near the fracture surface is evident in Figure 8a. The gouge is about 0.02-inches deep. Flowed metal beneath the gouge can be seen in Figures 8b and 8c. The most severely flowed metal seems to penetrate about 0.0006-inches below the bottom of the gouge. Away from the flowed metal, the microstructure has the usual appearance of a quenched and tempered steel. These observations --- a gouge, flowed metal beneath the gouge, and a typical quenched and tempered microstructure --- were found in Specimens II and III, also, indicating a reasonably uniform disturbance throughout the region shown in Figure 7. A crack in the bottom of the gouge was detected in the fracture profile of Specimen II, as shown in Figure 9.

Figure 10 shows rusted regions where paint is missing near the fracture origin. Some of these rusted regions are probably due to abrasion of paint during normal handling of the cylinder. Other rusted regions bear a striking resemblence to the temporary identification markings usually placed on the cylinder at the time of manufacture. For example, it is possible to discern "67) 114" in Figure 10. "67" is identical to the last two digits in the serial number --- T-0967 --- and "114" is identical to the tare weight noted for this cylinder on the Record of Hydrostatic Tests. The "114" can be seen in Figure 7 if it is turned upside down. These markings are known to develop when paint --- applied at the time of manufacture over temporary markings --- does not adhere at the location of the markings. It appears purely coincidental that these markings show up near the fracture origin.

4.2 Probable Fracture Path

It is helpful to imagine the as-received cylinder folded back into its original shape in order to discuss the probable fracture path. It is likely that two cracks moved out from the origin marked at a and a' in Figure 1b, one traveling toward the top and the other toward the bottom. Evidently, the crack which moved toward the top jumped the neck. A clean break is indicated by the relatively undamaged threads in the neck, Figure 11. After jumping the neck, this crack appeared to have traveled longitudinally toward the bottom and arrested in the 0.6-inch thick bottom.

The crack which moved toward the bottom branched three ways upon reaching the bottom, Figure 1b. One crack traveled radially in the bottom and arrested. A second crack traveled a short way circumferentially around the bottom and arrested. And the third crack traveled circumferentially a bit, then turned upward and followed a longitudinal path to an arrest point in the relatively thick neck.

4.3 Description of Fracture Mode

Ductile fracture seemed to be the only fracture mode for the longitudinal tears. This observation applies to the fracture origin, as well as to the regions of the fast-running crack. Ductile fracture was evidenced by the fibrous appearance of the fracture surface --- Figures 5, 6 and 11 --- as well as by wall thinning near the fracture surface. Wall thinning is evident in Figure 12, where the through-thickness fracture profile of Specimen I is shown. Measurements made on Figure 12 show that the wall thickness at the fracture surface is about 7% less than the wall thickness about 0.3-inches away from the fracture surface. Ductile fracture was also evidenced along the longitudinal tears by shear lips at about 45° to the longitudinal fracture plane, Figure 13.

There is no obvious explanation for the smooth surface of the step between the pair of unlinked, part-through cracks. The crack arrest point which appears under the step in Figure 4b may have developed when the step formed.

5. RESULTS OF METALLOGRAPHIC EXAMINATION

5.1 Observations of Fracture Profiles

Fracture profiles were examined in the region of the fracture origin using Specimens II, III and IV, as indicated in Figure 7. The objective was to look for differences between the features of the fracture profile along the rusty and discolored region which spanned 91% of the wall thickness, and along the unrusted, highly-reflective band spanning 9% of the wall thickness, as indicated in Figures 4 and 5. Typical results appear in Figure 14.

Figure 14a shows the full thickness fracture profile of Specimen IV. Figures 14b and 14c are close-ups of the regions indicated by the upper and lower arrows, respectively, in Figure 14a. In general, the fracture profile near the upper arrow showed rounded recesses and rounded dimples, which were coated with corrosion product. In the region indicated by the lower arrow, the fracture profile showed sharp recesses and pointed dimples. Similar observations were made on the full thickness fracture profiles of Specimens II and III. These results support the view that a part-through crack existed at the fracture origin. Evidently, the part-through crack had been exposed to a corrosive medium, but it is not possible to establish the time of exposure accurately.

3. Voids which have linked up appear next to the fracture profile in Figure 14b. The orientation of these voids suggests that they formed where inclusions of the type shown on face C of Figure 15 (See Section 5.2.1) separated from the steel matrix. The corrosion product in the voids, and also the rounded contours of the voids, suggest that they were connected to the fracture surface. The connection is not evident in Figure 14b, probably because of the way the metallographic section was cut. Perhaps these and other voids formed in response to local stresses which caused some shape distortion when the part-through crack formed.

5.2 Inclusions

5.2.1 Kind and Orientation

From metallographic observations in three directions, Figure 15, it was concluded that the kinds of inclusions present included manganese sulfide, silicates and titanium nitride. Intact inclusions elongated in the longitudinal direction are probably manganese sulfide inclusions. Fragmented inclusions strung out in the longitudinal direction are probably alumina inclusions. And those inclusions which appear as squares or rectangles are probably titanium nitride inclusions.

The orientation of inclusions in the gas cylinder wall is developed by the fabricating process. For example, the manganese sulfide inclusions are highly ductile at forging and drawing temperatures. Consequently, these inclusions are elongated into continuous platelets, with the longest axis in the longitudinal direction as is evident in Figures 15b and 15c. The second-longest axis of the platelet is in the circumferential direction, as is evident in Figures 15b and 15d. On the other hand, alumina and titanium dioxide inclusions are not ductile at forging and drawing temperatures, and consequently these inclusions are fragmented and strung out with the principal axis in the longitudinal direction, Figures 15b and 15c. Moreover, these more brittle inclusions are not readily flattened into platelets.

The orientation of all these kinds of inclusions has a strong influence on the direction in which cracks can run most readily. It is common for cracks to run along the interface between an inclusion and the steel matrix because the fracture energy along this interface is lower than the fracture energy of the steel matrix itself. Consequently, in a structure with predominantly longitudinal inclusions, longitudinal crack propagation will require less energy than circumferential crack propagation, and failure via longitudinal crack propagation will be assisted. Of course, the primary reason for longitudinal crack propagation in a cylindrical pressure vessel is the fact that the hoop stress is twice as large as the axial stress.

Circumferential crack propagation will be assisted by inclusions which are slightly extended in the circumferential direction and also by localized stresses associated with shape distortion. Measurements of the orientation dependence of the energy for crack propagation appear in Section 6.2

5.2.2 Inclusion Content

A quantitative estimate of the inclusion content was carried out as specified in ASTM Designation E 45-74 --- "Standard Recommended Practice For Determining the Inclusion Content of Steel."[4] Method A of this recommended practice was used on face A, Figure 15b, on a single specimen which was about 1/2 x 1-inches. Counts were made by two observers. Manganese sulfide and alumina inclusions were the principal types found. For this steel, titanium nitride inclusions were counted under the alumina classification. Manganese sulfide and alumina inclusions are designated as Type A and Type B inclusions, respectively, on the Jernkontoret chart cited in ASTM E 45-74. Inclusions are classified as thin or heavy. As shown in the following tabulation, only thin sulfide inclusions were found, whereas both thin and heavy alumina inclusions were found.

INCLUSION CONTENT RATED BY ASTM E 45-74 - METHOD A
(Based on worst field in 0.25 sq. inch specimen)

	Manganese Sulfide (Type A)		Alumina (Type B)	
	Thin	Heavy	Thin	Heavy
First Observer	3.60	--	1.25	1.25
Second Observer	3.67	--	1.67	--
Average	3.63	--	1.46	1.25

The ASTM scale of inclusion rating numbers ranges from 1 to 5, with 1 representing the lowest inclusion content. A rating number of 3 to 4 is not unusual for a steel with the concentrations of sulfur, phosphorus and oxygen shown in Tables I and II. Of particular interest in Table I is the observation that the sulfur concentration is the maximum permitted by specification DOT 3AA. The inclusion contents for classifications other than manganese sulfide and alumina inclusions, namely, silicate (Type C) and globular (Type D), were so low that they did not register on the ASTM scale.

5.3 Microhardness Measurements Near Gouge

In Figure 8, evidence of a 0.02-inch deep gouge and evidence of flowed metal beneath the gouge was shown for the fracture profile of Specimen IV. Two Knoop microhardness traverses were made on this metallographic specimen, along the lines labeled A and B in Figure 8a. The purpose of making these hardness measurements was to search for evidence of strain hardened metal beneath the gouge. To facilitate accurate measurement, hardness was measured using the Knoop microhardness technique. The range of Knoop hardness numbers measured, 257 to 313, corresponds roughly to Rockwell hardness numbers on the C-scale of 21 to 30.

A plot of hardness versus distance below the surface appears in Figure 16. The mid-thickness of the wall occurs at a depth of about 0.12-inches. It can be seen in Figure 16 that microhardness at depths between 0.01 - 0.03 below the surface as indicated in Figure 8a, is greater for traverse A than for traverse B. Below 0.03 inches, microhardness is about the same along both traverses. These results are interpreted as evidence of strain hardened metal beneath the gouge. They confirm that the metal had flowed when it was gouged.

5.4 Search For Evidence of Heating

In general, etched specimens of this gas cylinder steel developed a rather dark appearance, as shown in Figures 8 and 12. This type of etching is characteristic of a quenched and tempered steel, which is the heat treatment reportedly given to this cylinder at the time of manufacture. Had the cylinder been heated in the region from which these specimens were cut --- the region shown in Figure 7 --- some evidence would probably appear in the etched microstructure. For example, had an arc strike occurred or had weld metal been deposited in the fracture origin, a detectable change in the microstructure would have developed. Since such a change was not evident, it is inferred that heating of the cylinder wall to temperatures associated with arc strikes or welding did not occur.

5.5 Evidence of Decarburization

Incidental to the observation of the fracture profile is the observation of a decarburized layer along the inside cylinder wall. The layer shows up as the white region along the inside wall in Figures 8 and 12. Specimens I, II, III and IV each showed evidence of decarburization --- the layer was about 0.002 to 0.004 inches deep. This decarburized layer does not seem to be related to the fracture of the gas cylinder.

6. RESULTS OF TESTS NOT REQUIRED IN SPECIFICATION DOT 3AA

6.1 Quenching

Because of the widely-recognized susceptibility of intermediate manganese steel to quench cracking, some laboratory quenching tests were carried out in an attempt to evaluate the quench cracking behavior of the steel used in gas cylinder T-0967. Test specimen dimensions were about 1 1/2 x 3/4 x 1/4 - inches. Four specimens were austenitized in a salt bath at 1600°F for about 40 minutes. One specimen was quenched in oil at about 140°F, one in oil at room temperature, one in boiling water and one in ice water. The as-quenched specimens were examined visually for cracks --- none were found. To check further, the specimen receiving the most severe quench was sectioned for metallographic examination. No cracks were found in this section. It was concluded that quench cracking was not a likely source of defects, at least for

these small size specimens. Furthermore, results of the magnetic particle inspection reported in Section 3.2 indicated that quench cracks had not formed at the time of manufacture, when the whole gas cylinder was quenched.

6.2 Impact Tests

Impact tests were carried out to evaluate the toughness of the steel in gas cylinder T-0967. Toughness is basically a measure of the energy absorbed during fracture. High values of absorbed energy generally indicate a low susceptibility to brittle fracture.

Charpy test specimens were prepared according to ASTM Specification E 23-72.[5] The cylinder wall was not thick enough to allow machining full-size Charpy test specimens --- so half-size specimens were prepared. All specimens were machined from material which was flattened at room temperature in a press. Flattening was necessary because of the distorted condition of the as-received cylinder. Flattening also helped overcome the natural curvature of the cylinder. Specimen dimensions were 0.197 x 0.395 x 2.165 - inches. Notch depth was 0.089 - inches --- 0.010 - inches deeper than the standard ASTM notch depth. This slightly deeper notch resulted from a machining error.

Charpy test results appear in Figures 17 and 18. Absorbed energy for longitudinal and circumferential crack propagation appears in Figures 17a and 17b, respectively. Lateral expansion for longitudinal and circumferential specimen orientations is plotted in Figures 18a and 18b, respectively. The notch orientation and crack propagation direction are shown pictorially on each figure.

Results in Figures 17 and 18 show a transition from higher to lower values of toughness, starting at about -40°F. At and above 0°F, these results show that there is less resistance to longitudinal crack propagation than to circumferential crack propagation. The absorbed energy data show an increase in resistance by a factor of 3.6, and the lateral expansion data show an increase in resistance by a factor of 3.3. Hence, the manner in which gas cylinder T-0967 failed --- three full-length longitudinal tears --- is consistent with these results. As noted in Section 5.2.1, the primary reason for longitudinal crack propagation in a cylindrical pressure vessel is the fact that the hoop stress is twice as large as the axial stress.

In Table V, the energy absorbed by Charpy test specimens is compared with the energy requirements of the proposed ISO specification for gas cylinders. Comparison is made with the ISO specification simply because it is the only known seamless steel gas cylinder specification with Charpy test requirements. These requirements are exceeded substantially in the case of longitudinal specimen orientation - circumferential crack propagation. However, the energy requirement of the specification is not met in the case of circumferential specimen orientation - longitudinal crack propagation. These comparisons emphasize the importance of specifying notch orientation in Charpy testing.

6.3 Notched Tensile Tests

Tensile tests were carried out on notched specimens to evaluate the influence of a notch on ductility. Three test specimens were machined from material which was flattened at room temperature in a press. Flattening was necessary to overcome the distorted condition of the as-received cylinder.

Test specimens were of the same dimensions as those for the tensile specimens described in Section 3.3. However, each specimen had notches machined into the sides at the center of the gage length, as indicated in the footnote to Table V. A notch in a tensile specimen of this size constrains the specimen from deforming in the width direction. Such constraint results in multiaxial stresses, as is the case in a pressurized gas cylinder. This stress state is exaggerated in the presence of a part-through crack.

Test results appear in Table VI. Comparing ductility in Table VI with ductility in Table III shows a significant decrease for the notched specimens --- average reduction in area decreased from 48.8 to 9.7%. Another significant influence of the notch is evident when comparing strengths in Tables VI and III. The average notched tensile strength is 113,700 psi, as compared to the average unnotched tensile strength of 99,800 psi. These results are consistent with known influences of notches on uniaxial tensile test results, namely, a significant loss of ductility and an apparent increase in tensile strength. Since all specimens were flattened, it is unlikely that the process of flattening influenced the trends in these comparisons.

6.4 Tensile Tests on Circumferential Specimens

Tensile tests were carried out on specimens so oriented that their long axis was in the circumferential direction, rather than in the longitudinal direction, as is usual. The objective of these tests was to determine whether or not there was any influence of test specimen orientation on tensile properties. All specimens were machined from material which was flattened at room temperature in a press. Flattening was necessary to overcome the natural curvature of the cylinder as well as to overcome the distorted condition of the as-received cylinder. Dimensions of these test specimens were the same as those of the longitudinal specimens described in Section 3.3.

The average tensile and yield strengths in Table VII compare favorably with the average tensile and yield strengths in Table III. However, reduction in area and elongation show decreases of about 30 and 40%, respectively. Hence, there seems to be no orientation dependence for strength, but a substantial dependence for ductility. This reduction in ductility is attributable in part to the inclusions elongated in the longitudinal direction, Figure 15.

The circumferential ductility shown in Table VII, 20% elongation, compares favorably with the circumferential ductility required in the flattening test, section 178.37-17(a) of specification DOT 3AA, which is 14-18%, as calculated from anvil separation, cylinder diameter and wall thickness.

7. STRESS ANALYSIS VIA FRACTURE MECHANICS

7.1 Background

Fracture mechanics is a field of stress analysis which evaluates the influence of cracks on the stress which a structure can safely support. The development of this field during the last thirty years resulted from the widespread recognition that most engineering structures may contain cracks which could lead to failure at applied stresses well below the yield stress. The utility of fracture mechanics lies in its ability to predict critical crack sizes in terms of applied stress and resistance to crack propagation. A structure with cracks below the critical size would remain intact, whereas a structure with larger cracks would fail.

Fracture mechanics measures the ability of a material to resist crack propagation in terms of "fracture toughness," signified by "K_{Ic}" for plane strain conditions, and "K_c" for plane stress, and with units of psi - $\sqrt{\text{inches}}$. Typical values of fracture toughness for steels range between 50,000 and 400,000 psi - $\sqrt{\text{inches}}$. Typical aluminum alloys exhibit fracture toughnesses in the range, 20,000 - 100,000 psi - $\sqrt{\text{inches}}$. Fracture toughness can be measured on precracked test specimens in an ordinary tensile testing machine. ASTM Standard Method E 399 - 72[6] describes plane strain fracture toughness testing of metallic materials.

The application of fracture mechanics to pressure vessels facilitates the prediction of stability, leaking, or catastrophic fracture in terms of fracture toughness, crack size and applied stress. The application of fracture mechanics to thin-walled cylindrical shells made from ductile metals, e.g., pipe, gas cylinders, is presently in the early stages of development.[7-9]

As regards gas cylinder T-0967, it was reported that the cylinder burst during a filling operation at a pressure of about 2500 psi. (See Section 1.2). This pressure is significantly less than the design burst pressure, estimated as 5100 psi by multiplying the marked filling pressure by the appropriate safety factor, 2.25. Results from this investigation show that the probable cause of this discrepancy between the design and actual burst pressures was a pair of closely-spaced, part-through cracks, as shown in Figures 4 and 5. The overall length is 3 inches, and the depth is 0.232-inches, which is about 91% of the wall thickness. One crack is 2 1/2-inches long, and the other is 1/2-inch long. The step, which is about 3/16-inches high, appears in Figure 6. The non-fibrous fracture surface of the step suggests that it did not form when the

fibrous fracture surfaces of the part-through cracks and the fast-running cracks formed. Hence, it is assumed that the step formed during the catastrophic rupture of the gas cylinder.

The cracks have a definite elliptical shape at the end away from the step. This shape is a widely-recognized characteristic of part-through cracks.[10] Judging from the depth of the cracks, it is likely that the cracks were sharp at the bottom rather than blunt. Furthermore, metallographic evidence from the part-through crack surfaces indicates that the fracture was ductile. The fracture in the region of the fast-running crack which developed at temperatures near or somewhat above room temperature, was also ductile. (See Section 4.3). The observed ductile mode of fracture is consistent with the impact data in Section 6.2, which show that this steel is on the upper shelf at temperatures above 0°F.

7.2 Hoop Stress At Failure

The following fracture mechanics evaluation of gas cylinder T-0967 is based on the empirical analysis of Maxey[8]. This analysis was developed for pipe with yield strengths from 40,000 to 70,000 psi, but it can be applied to other tubular products which are approximately in this yield strength range, including gas cylinders. As a starting point, Maxey[8] (and others)[7,9] point out that stress magnification will occur at the ends of a crack. Consequently, plastic flow and fracture can occur at nominal applied wall stresses lower than the yield strength. In the case of a longitudinal crack in the sidewall of a gas cylinder, stress magnification is due to redistribution of the hoop stress around the crack and to bending moments caused by bulging near the crack.

The stress magnification factor due to bulging of tubular products containing a through-wall, axial defect, M_T, was developed by Folias[11] and is given by

$$M_T = \left(1 + 1.255 \frac{c^2}{RT} - 0.0135 \frac{c^4}{R^2 t^2}\right) 1/2 \qquad (1a)$$

For the case of a part-through axial crack, the stress magnification factor, M_P, is estimated by Maxey[8] as

$$M_P = (1 - d/M_T t)/(1 - d/t) \qquad (1b)$$

In the above equations,

d = depth of a part-through crack

2c = length of a through-wall crack

R = cylinder radius

t = wall thickness

2c' = equivalent crack length in the case of a part-through crack with non-rectangular ends

and M_T' is calculated using c' in equation 1a.

The stress magnification factor shows up in the equations used to calculate the hoop stress at failure. Equations have been defined by Maxey[8] for two types of fractures, classified as "flow stress controlled" (plastic behavior) and "toughness controlled" (elastic-plastic behavior). Equations for both types of behavior appear below.

In the case of a through-wall, axial crack, the equation for toughness-controlled behavior, $_T$, is as follows:

$$\ell n \sec \frac{\pi}{2} (M_T \sigma_T / \sigma_f) = K_c^2 \pi / (8c\sigma_f^2) = 12E\pi(C_v/A_c)/(8_c\sigma_f^2) \qquad (2a)$$

For a through-wall defect, the equation for flow stress controlled behavior is

$$\sigma_T^* = \sigma_f / M_T \qquad (2b)$$

In the case of a part-through axial crack, the hoop stress at failure for toughness-controlled behavior, σ_P, is given by

$$\ell n \sec \frac{\pi}{2} (M_P \sigma_P / \sigma_f) = K_c^2 \pi / (8c' \sigma_f^2) = 12E\pi(C_v/A_c)/(8_c\sigma_f^2) \qquad (3a)$$

whereas for flow stress controlled behavior, the equation is

$$\sigma_P^* = \bar{\sigma} / M_P. \qquad (3b)$$

In the above equations σ_T, σ_P = hoop stress at failure for toughness controlled behavior,

σ_T^*, σ_P^* = hoop stress at failure for flow stress controlled behavior

σ_f = the flow stress of the steel (assumed by Maxey and others to be yield strength + 10,000 psi)

K_c = plane stress fracture toughness of material

C_V/A_C = impact energy per unit area of a Charpy test specimen (half size or full size)

E = Young's modulus (30×10^6 psi)

$2c$ or $2c'$ = the length of the crack

M_T = stress magnification factor given by Equation 1a

M_P = stress magnification factor given by Equation 1b

Stress analysis cannot be easily carried out for the case of the two closely-spaced, but separate cracks shown in Figures 4 and 5. Hence, to estimate upper and lower bounds for the hoop stress at failure, calculations were made for the actual 2 1/2-inch long crack and for an assumed 3-inch long crack. Because of the depth of the part-through crack, 91% of the wall thickness, determination of c' rather than c for calculating M_p was considered an unnecessary refinement. Results appear in Table VIII, where the first column shows that the stress magnification factor is larger for the part-through crack than for the full through crack. The second column shows a factor based on the Charpy test results which is used to classify the fracture as toughness controlled or flow stress controlled. Maxey indicates that values of this factor less than 4, as appearing in the table, mean that the fracture is toughness controlled. Thus, Equations 2a and 3a were used to calculate the hoop stresses at failure, which appear in the third column. Values of the parameter, $M\sigma/\sigma_f$, which appear in the fourth column, also show that the fracture was slightly toughness controlled.

In the case of the part-through crack, failure means that the ligament beneath the part through crack ruptured, and a full-through crack formed. At this point, results in Table VIII suggest that the cylinder simply leaked, because the ligament ruptured at a hoop stress of 12,200 to 20,200 psi, which is less than the stress required for the full-through crack to run catastrophically, namely, 38,100 to 54,300 psi. Continued filling of the leaking cylinder to the allowable filling pressure would have developed hoop stresses in this range. For example, the hoop stress estimated from the reported gas pressure at burst,

$\sigma_B = PR/t = 2500 \times 4.28/0.256 = 41{,}800$ psi, falls in this stress range.

7.3 Estimation of Fracture Toughness

The plane stress fracture toughness of the quenched and tempered steel in gas cylinder T-0967 can be estimated from Maxey's[8] empirical correlation

$$K_c = \sqrt{12\ E\ C_v/A_c} \qquad (4)$$

where the terms have the meanings defined in Section 7.2. The estimated fracture toughness is orientation dependent, due to the orientation dependence of the Charpy values shown in Table V. Fracture toughness values appear in Table IX. These values compare favorably with other plane stress values reported for quenched and tempered steels of similar yield strength.[12]

8. DISCUSSION

Results in Section 3 demonstrate that the material in gas cylinder T-0967 conformed to the requirements of specification DOT 3AA, in matters of chemistry, resistance to crack formation during quenching, strength and ductility. One notable feature in the chemistry is that the sulfur concentration was at the maximum allowable, leading to the maximum content of manganese sulfide inclusions, which are known to lower crack propagation resistance. Another notable feature in the chemistry is the relatively high titanium content, which suggests the possibility of deoxidation with titanium rather than with the more traditional elements, aluminum and silicon. Magnetic particle inspection did not reveal any cracks in the as-received cylinder. Furthermore, it was found that quench cracks could not be developed in small test specimens which were given a severe quench in ice brine. Ductility exceeded specification requirements significantly.

Minimum tensile strength in Table III and minimum wall thickness in Table IV are such that the calculated hoop stress at test pressure, 65,800 psi, exceeded by about 2 percent, the allowable hoop stress, .67 x 96,800 = 64,500 psi, as defined in section 178.37-10(b) of specification DOT 3AA. Hence, this strength requirement was not met. This observation is consistent with the hydrostatic test report, which indicates a rather high permanent expansion for gas cylinder T-0967, as compared with other cylinders in the same heat treatment lot. As a matter of general interest, it is noted that the calculated hoop stress at test pressure, does not exceed the value of .67 x 99,800 = 66,900 psi, which is obtained by taking 67 percent of the average tensile strength reported in Table III.

The burst of gas cylinder T-0967 during filling seems traceable to the presence of two unlinked, but closely-spaced part-through cracks which were located about 10-inches below the neck. These cracks penetrated about 91% of the wall thickness. They appeared to be related to a surface disturbance which was evidenced by a gouge, lips of raised metal and strain hardened metal close to the surface. The part-through cracks, the gouge, and the lips of raised metal suggest that the cylinder received an impact of mechanical origin. Furthermore, the rust appearance of the fracture surfaces of the part-through cracks and the rust on the damaged exterior surface near the cracks suggest that the cracks were present at the time the cylinder was being filled. That the reported burst pressure was much lower than the design burst pressure also suggests that the defects were present at the time of filling.

From a fracture mechanics analysis of the cylinder containing a part-through crack, it was inferred that the ligament beneath the part-through cracks ruptured during filling at a hoop stress between 12,200 and 20,200 psi. It was also inferred that the cylinder leaked while filling continued, until a critical hoop stress between 38,100 and 54,300 psi was reached, at which stress the full-through crack ran catastrophically and ultimately formed three full-length longitudinal tears. The uncertainty in the hoop stresses at which rupture occurred

arises because the step in the part-through crack makes precise analysis difficult. Nevertheless, the hoop stress estimated from the reported gas pressure at burst, 41,000 psi, falls in this stress range. Protection against catastrophic crack propagation can be designed into a gas cylinder by developing sufficient fracture toughness to resist extension of the largest expected defects at operating pressures. The observed low strength of gas cylinder T-0967 would not have affected its catastrophic failure via longitudinal tears unfavorably. In fact, a trend toward lower strength usually signifies increasing fracture toughness, and thus, increasing resistance to fracture.

Ductile fracture seemed to be the only mode of fracture for the longitudinal tears. This observation applies to the fracture origin, as well as to the region of the fast-running crack. There is no obvious explanation for the smooth surface of the step between the pair of unlinked, part-through cracks.

Results of impact tests on Charpy specimens showed that longitudinal crack propagation required significantly less energy than did circumferential crack propagation. This result is attributable to the rather high concentration of sulfide inclusions elongated in the longitudinal direction. The absorbed energy for circumferential crack propagation exceeded the requirement in a proposed ISO specification. However, no requirement was defined in that specification for longitudinal crack propagation, which was the principal crack propagation direction in the pneumatically-burst gas cylinder. This behavior, and the observation of a lower energy for longitudinal crack propagation, demonstrate the importance of recognizing the orientation-dependence of mechanical properties.

Notched tensile specimens showed a substantial loss in reduction in area, as compared to smooth tensile specimens. This observation suggests that notch sensitivity is an important characteristic of this quenched and tempered carbon-manganese steel.

Tensile test results on circumferential specimens were similar to results on longitudinal specimens in the matter of yield and tensile strengths. Ductility of the circumferential specimens was significantly lower, but still compared favorably with the circumferential ductility required in the whole-cylinder flattening test. These observations demonstrate once again the importance of recognizing the orientation-dependence of mechanical properties.

9. CONCLUSIONS

1. The material in gas cylinder T-0967 conformed to the requirements of specification DOT 3AA in matters of chemistry, resistance to crack formation during quenching, and ductility.

2. The material in gas cylinder T-0967 did not conform to the requirements of specification DOT 3AA in matters of tensile strength and wall thickness. Minimum tensile strength and minimum wall thickness

were such that the calculated hoop stress at test pressure exceeded the allowable hoop stress by about 2.0%. This strength consideration would not cause an unfavorable effect on the fracture toughness of the material.

3. The burst of gas cylinder T-0967 during filling seems traceable to the presence of two unlinked, but closely-spaced part-through cracks which were located about 10-inches below the neck. The cracks probably resulted from an impact of mechanical origin and probably were present at the time the cylinder was being filled.

4. Results of impact tests on Charpy specimens showed that longitudinal crack propagation required significantly less energy than did circumferential crack propagation.

5. Results of tensile tests showed that longitudinal test specimens exhibited significantly greater ductility than did circumferential test specimens.

6. Results of tests on notched tensile specimens indicate that notch sensitivity is an important characteristic of quenched and tempered carbon-manganese steel.

10. ACKNOWLEDGEMENTS

Mr. C. H. Brady obtained documentation photographs and conducted the metallographic work. Magnetic particle testing was done by Mr Mr. T. R. Shives. Mr. L. Smith, Mr. T. P. Royston and Mr. W. A. Willard assisted in mechanical testing and in the preparation of the manuscript. Mr. G. Hicho provided assistance with the inclusion counting, and Mr. Hicho and Dr. C. G. Interrante assisted with the fracture mechanics analysis. Mr. A. Mallen and Mr. P. Seay contributed several helpful discussion during the course of this work.

REFERENCES

1. Preliminary Reports on Pneumatically Burst Gas Cylinder From NBS Mechanical Properties Section to Office of Hazardous Materials Operations - Department of Transportation.

   a. September 26, 1975. "Thickness Measurements of Seamless Steel Gas Cylinder T-0967," memo report from B. W. Christ to P. Seay, OHMO-DOT.

   b. December 10, 1975. "Results of Tensile Tests on 3AA Seamless Cylinder No. T-0967," memo report from J. H. Smith to A. J. Mallen, OHMO-DOT.

   c. January 22, 1976. "Evaluation of Steel Gas Cylinder T-0967," memo report from B. W. Christ to A. J. Mallen, OHMO-DOT.

   d. June 18, 1976. "Preliminary Report on Pneumatically Burst Gas Cylinder T-0967," memo report from B. W. Christ to A. J. Mallen, OHMO-DOT.

2. Specification DOT 3AA Code of Federal Regulations, Title 49. Transportation, p. 418, 1975. U.S. Government Printing Office, Washington, D.C. 20402.

3. American Iron and Steel Institute (AISI) Steel Products Manual.

   a. Carbon Steel: Semifinished for Forging; Hot Rolled and Cold Finished Bars; Hot Rolled Deformed Concrete Reinforcing Bars.

   b. Alloy Steel: Semifinished; Hot Rolled and Cold Finished Bars.

4. ASTM E 45-74, "Standard Recommended Practice For Determining the Inclusion Content of Steel," American Society for Testing and Materials, 1916 Race Street, Philadelphia, Pennsylvania 19103.

5. ASTM E 23-72, "Standard Methods For Notched Bar Impact Testing of Metallic Materials," American Society For Testing and Materials, 1916 Race Street, Philadelphia, Pennsylvania 19103.

6. ASTM E 399-72, "Standard Method of Test For Plane Strain Fracture Toughness of Metallic Materials," American Society For Testing and Materials, 1916 Race Street, Philadelphia, Pennsylvania 19103.

7. D. Broek: "Fracture of Structures - Pressure Vessels and Piping," Chapter 15.2 of Elementary Engineering Fracture Mechanics, Noordhoff International Publishing, Leyden, The Netherlands, 1974.

8. W. A. Maxey: "Fracture Initiation, Propagation and Arrest," pp. J-1 to J-31 in Fifth Symposium on Line Pipe Research, Pipeline Research Committee of American Gas Association, Houston, November, 1974.

9. F. Erdogan: "Ductile Fracture Theories For Pressurized Pipes and Containers," The International Journal of Pressure Vessels and Piping, Vol. 4, pp. 253 - 283, October, 1976.

10. The Surface Crack: Physical Problems and Computational Solutions, J. R. Swedlow, Editor. The American Society of Mechanical Engineers 345 East 47th Street, New York 10017. 1972.

11. E. S. Folias: "The Stresses in a Cylindrical Shell Containing an Axial Crack," ARL 64-174, Aerospace Research Laboratories (1964).

12. A. M. Sullivan and J. Stoop: "Some Fracture Mechanics Relationships for Thin Sheet Materials," NRL Report 7650, December 21, 1973. Strength of Materials Branch, Metallurgy Division, Naval Research Laboratory, Washington, D.C.

LIST OF FIGURE CAPTIONS

1a. Overall view of pneumatically burst gas cylinder, showing both halves of the neck. An intact cylinder is included for comparison.

1b. Overall view of pneumatically burst gas cylinder, showing the bottom. Regions a and a' indicate the fracture origin.

2a. View of Department of Transportation stampings on neck of gas cylinder T-0967. Note the crack arrest in this half of the neck.

2b. View of identifying stampings on neck half of gas cylinder T-0967 opposite to that shown in Figure 2a.

3. Markings on the bottom of cylinder T-0967, showing the heat code, V18.

4a. View of fracture surface showing the side of the fracture origin labeled a' in Figure 1b. The elliptical ends of the fracture origin and the bright region along the inside wall are characteristic features of a part-through crack.

4b. View of the same side of the fracture origin shown in Figure 3a. Note the step in the fracture surface and the lips of raised metal on the external surface.

5. View of the side of the fracture origin labeled a in Figure 1b, with a schematic diagram showing dimensions.

6. The stepped region of the fracture origin, contrasting the smoothness of the step with the fibrous nature of the adjacent fracture surface.

7. Mating halves of the fracture origin placed together to give an approximate picture of the configuration before burst.

8. Fracture profile of Specimen IV in Figure 7. (a) Gouge in outside wall at fracture profile. (b) and (c) Evidence of flowed metal beneath gouge.

9. Fracture profile of Specimen II in Figure 7, showing a gouge with a crack in the bottom.

10. Rusted regions on the external surface near the fracture origin.

11. Fracture surface near neck of cylinder, showing fibrous fracture and relatively undamaged threads.

12. Fracture profile of Specimen I in Figure 7, showing wall thinning near the fracture surface.

13. Cross-section through wall in region of fast-running crack, showing shear lip.

14. Fracture profile of Specimen IV in Figure 7. (a) Full-thickness profile. (b) Corrosion product and rounded recesses in rusty and discolored region of fracture origin. (c) Sharp recesses and pointed dimples in the bright region along the inside wall below the fracture origin.

15. Inclusions (a) Schematic representation and nomenclature (b) Inclusions as seen on Face A in Figure 15a. (c) Inclusions as seen on Face B in Figure 15a. (d) Inclusions as seen on Face C in Figure 15a.

16. Knoop hardness versus distance below surface for the fracture profile of Specimen IV in Figure 7.

17a. Absorbed energy versus temperature for longitudinal crack propagation.

17b. Absorbed energy versus temperature for circumferential crack propagation.

18a. Lateral expansion versus temperature for longitudinal crack propagation.

18b. Lateral expansion versus temperature for circumferential crack propagation.

LIST OF TABLES

TABLE I

CHEMICAL COMPOSITION

Element	Results* From Gas Cylinder Number T-0967 (weight percent)	Requirements of Specification DOT 3AA For Intermediate Manganese Steel	
		Ladle Analysis (weight percent)	Check Analysis (weight percent)
Carbon	0.34	0.40 max	+0.03/-0.02
Manganese	1.44	1.35/1.65	±0.05
Phosphorus	0.019	0.04 max	+0.01
Sulfur	0.050	0.05 max	+0.01
Silicon	0.27	0.10/0.30	+0.03/-0.02

* Chemical analysis carried out by Chicago Spectro Laboratory, Chicago, Illinois.

TABLE II

RESIDUAL ELEMENTS

Element	Results* From Gas Cylinder T-0967 (Weight Percent)	AISI Maximum Limits of Residual Elements (Reference 3) (Weight Percent)
Copper	0.17	0.35
Nickel	0.13	0.25
Chromium	0.13	0.13
Molybdenum	0.02	0.06
Titanium	0.03	+
Aluminum	0.03	+
Nitrogen	0.013	+
Oxygen	0.015	+

* Chemical analysis carried out by Chicago Spectro Laboratory, Chicago, Illinois.

\+ Unspecified.

TABLE III

TENSILE TEST RESULTS ON LONGITUDINAL TEST SPECIMENS*

Specimen Number	Percent Elongation in 2-inches	Percent Reduction in Area	Tensile Strength (psi)	0.2% Offset Yield Strength (psi)
TL 1	29.5	44.0	100,500	73,000
TL 2	26.6	50.4	96,800	73,100
TL 3	28.5	50.0	101,000	79,900
TL 4	28.0	50.6	101,600	76,800
Average	28.2	48.8	99,800	75,700

* Nominal Test Specimen Dimensions:

Gage Length	2.0-inches
Gage Width	1.5-inches
Gage Thickness	0.25-inches

TABLE IV

Wall Thickness Measurements

Connection Ribbon Section

Bottom Longitudinal Crack Arrest Side (B)		Top Longitudinal Crack Arrest Side (C')	
Near top	0.230 inches	Near top	0.239 inches
	0.220		0.228
	0.224		0.230
	0.227		0.225
Near bottom	0.241		0.242
		Near bottom	0.241

Section Connected to Bottom

Bottom Longitudinal Crack Arrest Side (B')		Bottom Circumferential Crack Arrest Side (With Gouge (A')	
Near top	0.230 inches	Near top	0.249 inches
	0.229		0.258 just above origin
	0.229		0.257 just below origin
	0.234		0.252
Near bottom	0.239		0.251
			0.253
			0.254
		Near bottom	0.260

Section With Top Crack Arrest

Side Opposite Gouge (A)		Top Longitudinal Crack Arrest Side (C)	
Near top	0.248 inches	Near top	0.235 inches
	0.255		0.227
	0.257 just above origin		0.228
	0.255 just below origin		0.235
	0.253		0.238
	0.253		0.240
	0.249	Near bottom	0.245
	0.243		
Near bottom	0.250		

Typical Bottom Thickness Measurements: 0.659, 0.654, 0.637-inches.

TABLE V

Comparison of Charpy Impact Test Results on Gas Cylinder T-0967
With Requirements of Proposed ISO Specification

Test Temperature	Absorbed Energy							
	Gas Cylinder T-0967*				Proposed ISO Specification** for Quenched and Tempered Carbon Manganese Steel (Specimen Width over 5 mm)			
	Circumferential Specimen Orientation Longitudinal Crack Propagation		Longitudinal Specimen Orientation Circumferential Crack Propagation		Longitudinal Specimen Orientation Circumferential Crack Propagation			
					Mean of 3 Specimens		Individual Specimen	
	joules/cm^2	(ft-lb)/in^2	joules/cm^2	(ft-lb)/in^2	joules/cm^2	(ft-lb)/in^2	joules/cm^2	(ft-lb)/in^2
0°C (32°F)	21.8	100	78.2	372.2	33	151	26	124

* At 0°C, these test results are on the upper shelf. Average of two test results.

** International Standards Organization, Technical Committee 58, Subcommittee 3 (Secretariat 104), Document 339, April, 1975.

TABLE VI

NOTCHED TENSILE TEST RESULTS ON
LONGITUDINAL TEST SPECIMENS*

Specimen Number	Percent Reduction in Area	Tensile Strength (psi)
NL-1	6.0	116,700
NL-3	8.0	111,400
NL-4	15.0	113,100
Average	9.7	113,700

* Nominal Test Specimen Dimensions:

Gage Length	2.0 - inches
Gage Width	0.75 - inches
Gage Thickness	0.25 - inches
Notch Depth	0.375 - inches
Root Radius of Notch	0.001 - inches, max.
Notch Angle	60°

TABLE VII

TENSILE TEST RESULTS ON CIRCUMFERENTIAL TEST SPECIMENS*

Specimen Number	Percent Elongation in 2-inches	Percent Reduction in Area	Tensile Strength (psi)	0.2% Offset Yield Strength psi
TT 1	**	**	101,000	79,500
TT 2	20	31	99,300	79,400
Average	--	--	100,200	79,500

* Nominal Test Specimen Dimensions:

Gage Length	2.0 - inches
Gage Width	1.5 - inches
Gage Thickness	0.25 - inches

** The specimen fractured outside the gage length near a surface defect. Meaningful ductility measurements could not be obtained.

TABLE VIII

RESULTS OF STRESS ANALYSIS FOR
AXIAL, PART-THROUGH CRACKS

Type and Length of Crack		Stress Magnification Factor	$K_C^2\pi/8c\sigma_f^2 = [12E\pi(C_V/A_C)]/8c\bar{\sigma}^2$	Hoop Stress at Failure (Toughness Controlled) (psi)	$\frac{M\sigma}{\bar{\sigma}}$
Part-Through	2.5-inches	$M_P = 3.74$	1.41	$\sigma_P = 20,200$	0.84
	3.0-inches	$M_P = 5.88$	1.18	$\sigma_P = 12,200$	0.80
Full-Through	2.5-inches	$M_T = 1.39$	1.41	$\sigma_T = 54,300$	0.84
	3.0-inches	$M_T = 1.88$	1.18	$\sigma_T = 38,100$	0.80

TABLE IX

PLANE STRESS FRACTURE TOUGHNESS OF
QUENCHED AND TEMPERED CARBON-MANGANESE
STEEL* INFERRED FROM HALF-SIZE CHARPY SPECIMENS

Crack Propagation Direction	Charpy Energy ($ft\text{-}lb/in^2$)	$K_c = (12E\ C_V/A_C)^{1/2}$ psi - $\sqrt{inches}$
Longitudinal	100	190,000
Circumferential	372	366,000

* Tensile Strength = 99,800 psi

COLOR - NO #

Figure 1a. Overall view of pneumatically burst gas cylinder, showing both halves of the neck. An intact cylinder is included for comparison.

Figure 1b. Overall view of pneumatically burst gas cylinder, showing the bottom. Regions a and a' indicate the fracture origin.

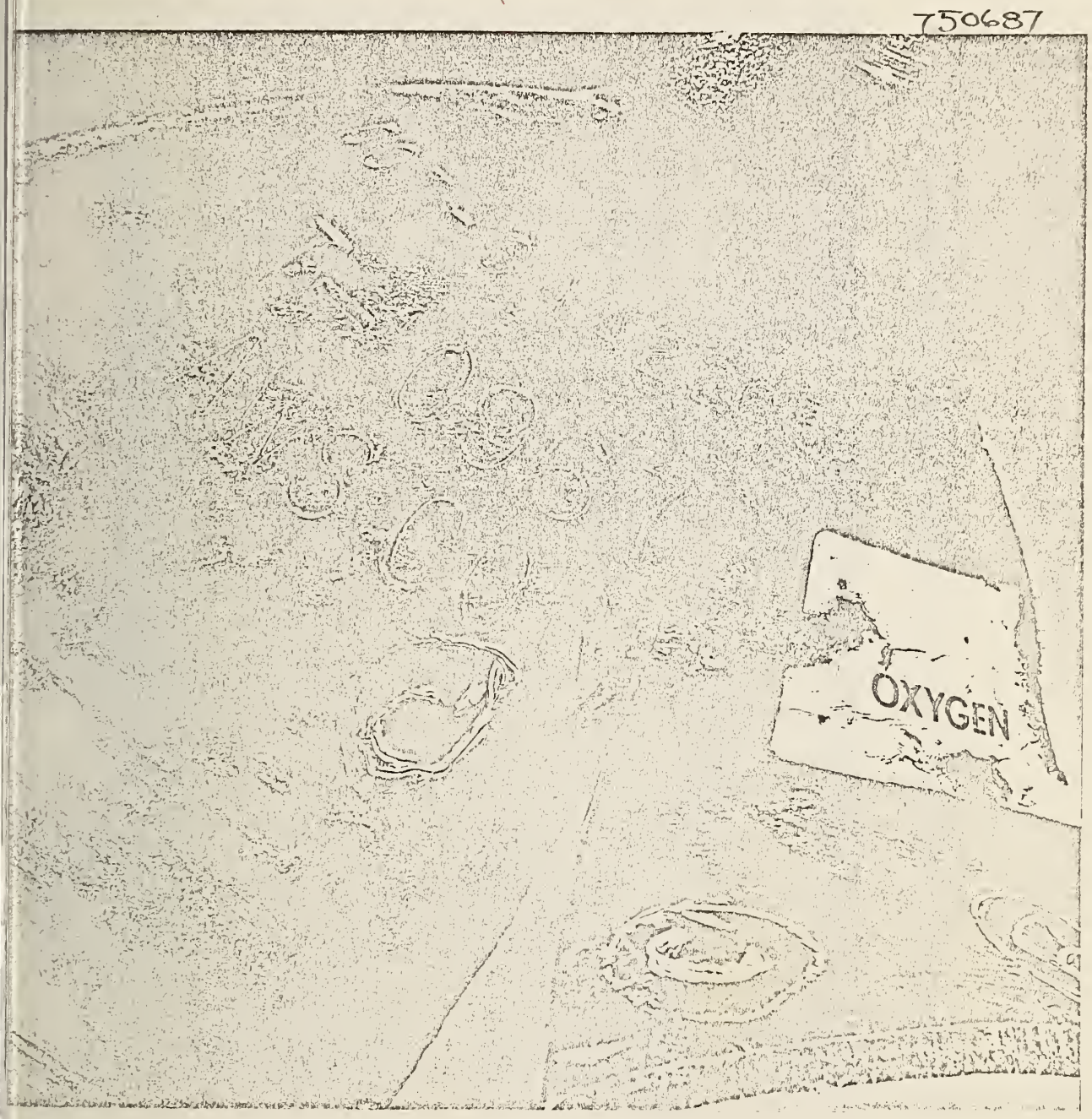

Figure 2a. View of Department of Transportation stampings on gas cylinder T-0967. Note the crack arrest in this half of the neck. X 1

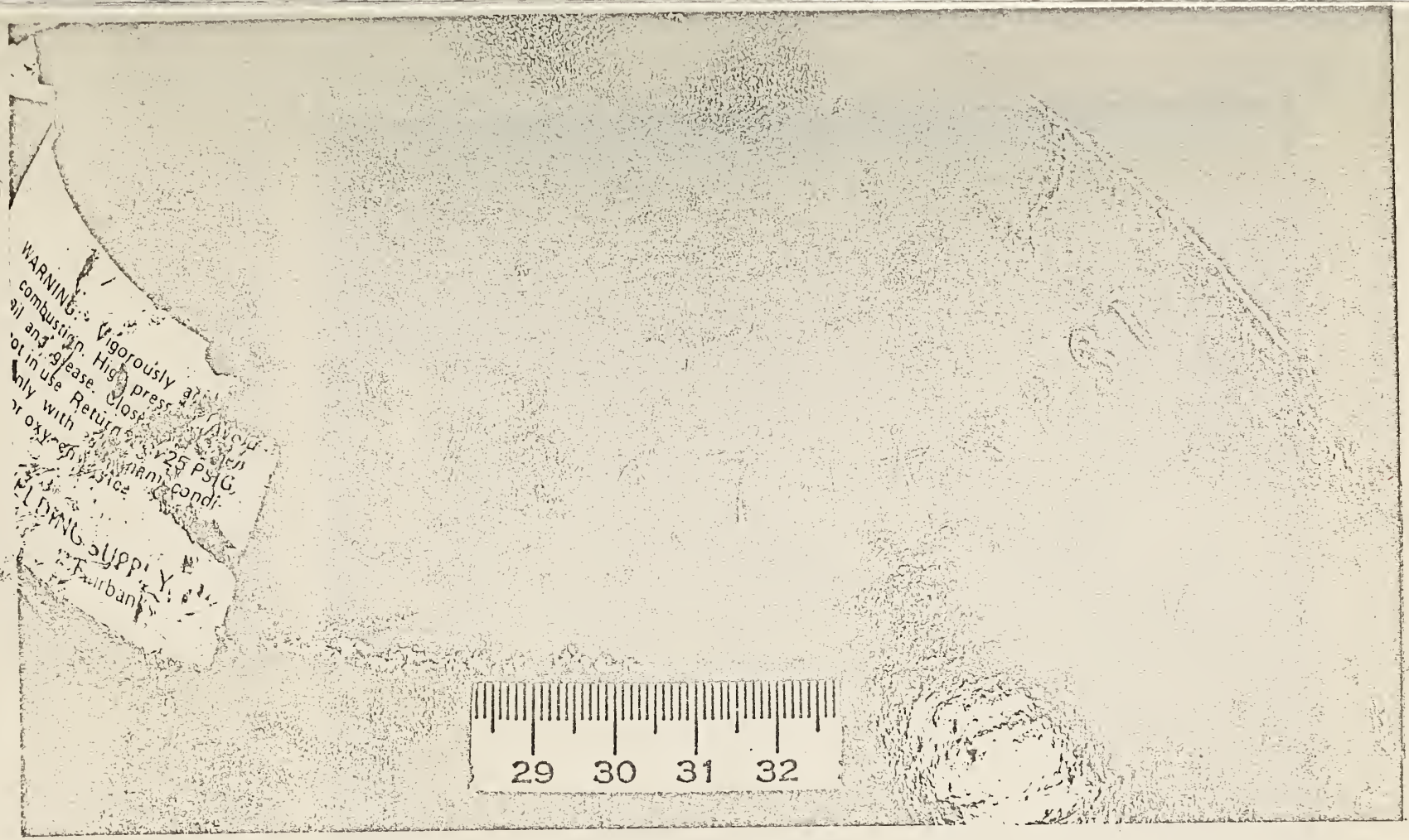

Figure 2b. View of identifying stampings on neck half of gas cylinder T-0967 opposite to that shown in Figure 2a. X 1

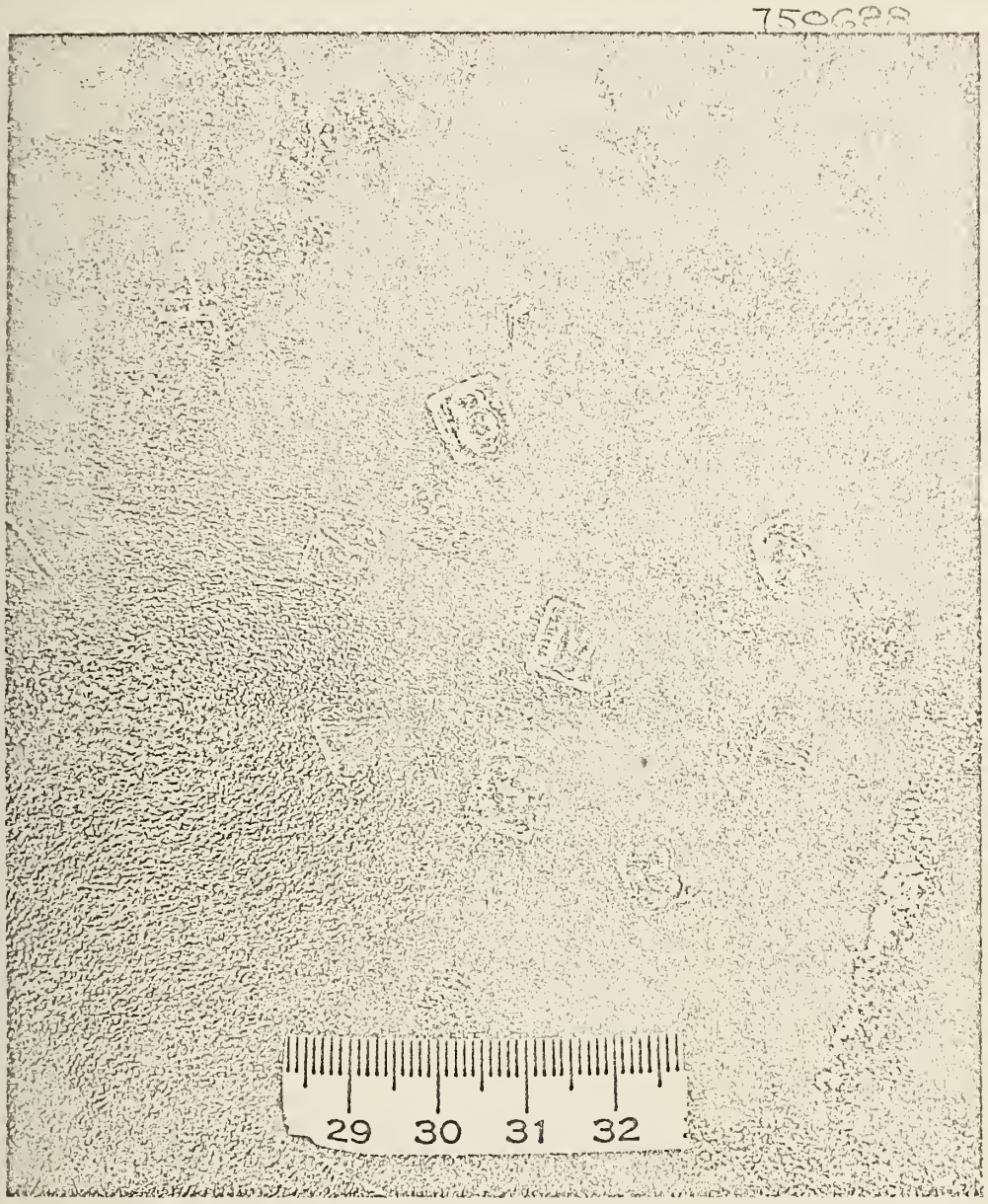

Figure 3. Markings on the bottom of cylinder T-0967, showing the heat code, V18. X 1

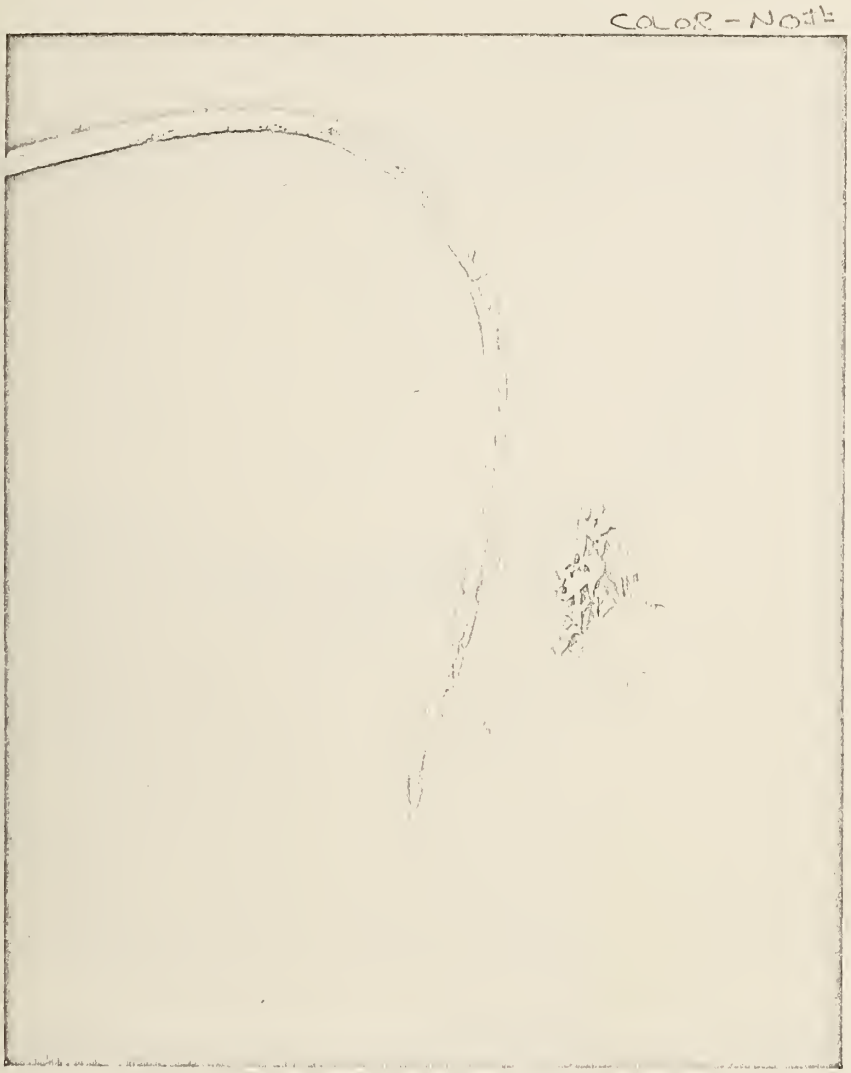

Figure 4a. View of fracture surface showing the side of the fracture origin labeled a' in Figure 1b. The elliptical ends of the fracture origin and the bright region along the inside wall are characteristic features of a part-through crack.

Figure 4b. View of the same side of the fracture origin shown in Figure 4a. Note the step in the fracture surface and the lips of raised metal on the external surface.

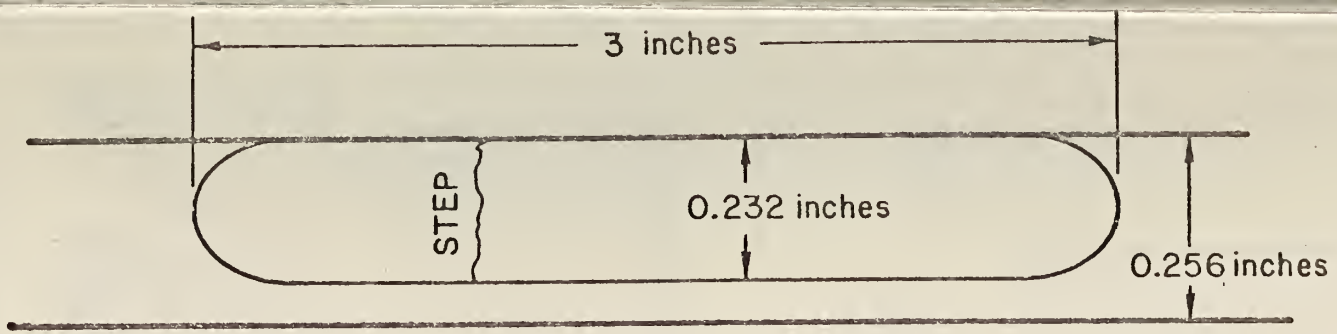

Figure 5. View of the side of the fracture origin labeled a in Figure 1b, with a schematic diagram showing dimensions.

Figure 6. The stepped region of the fracture origin, contrasting the smoothness of the step with the fibrous nature of the adjacent fracture surface. X 4

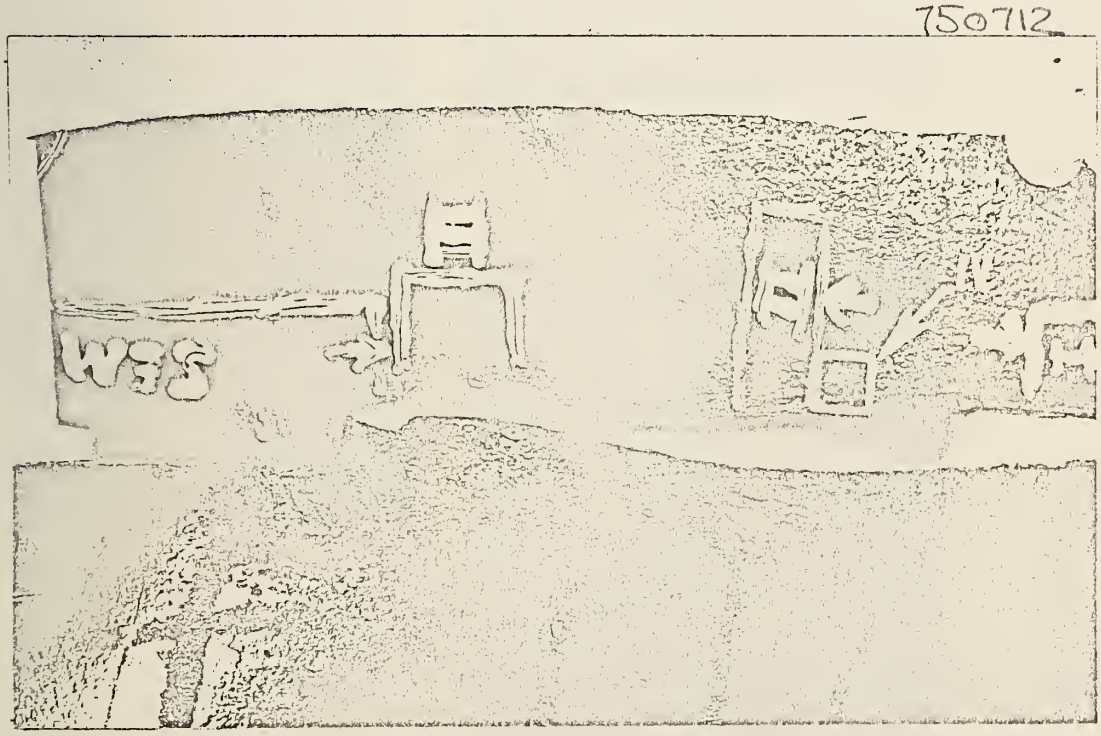

Figure 7. Mating halves of the fracture origin placed together to give an approximate picture of the configuration before burst. X 1

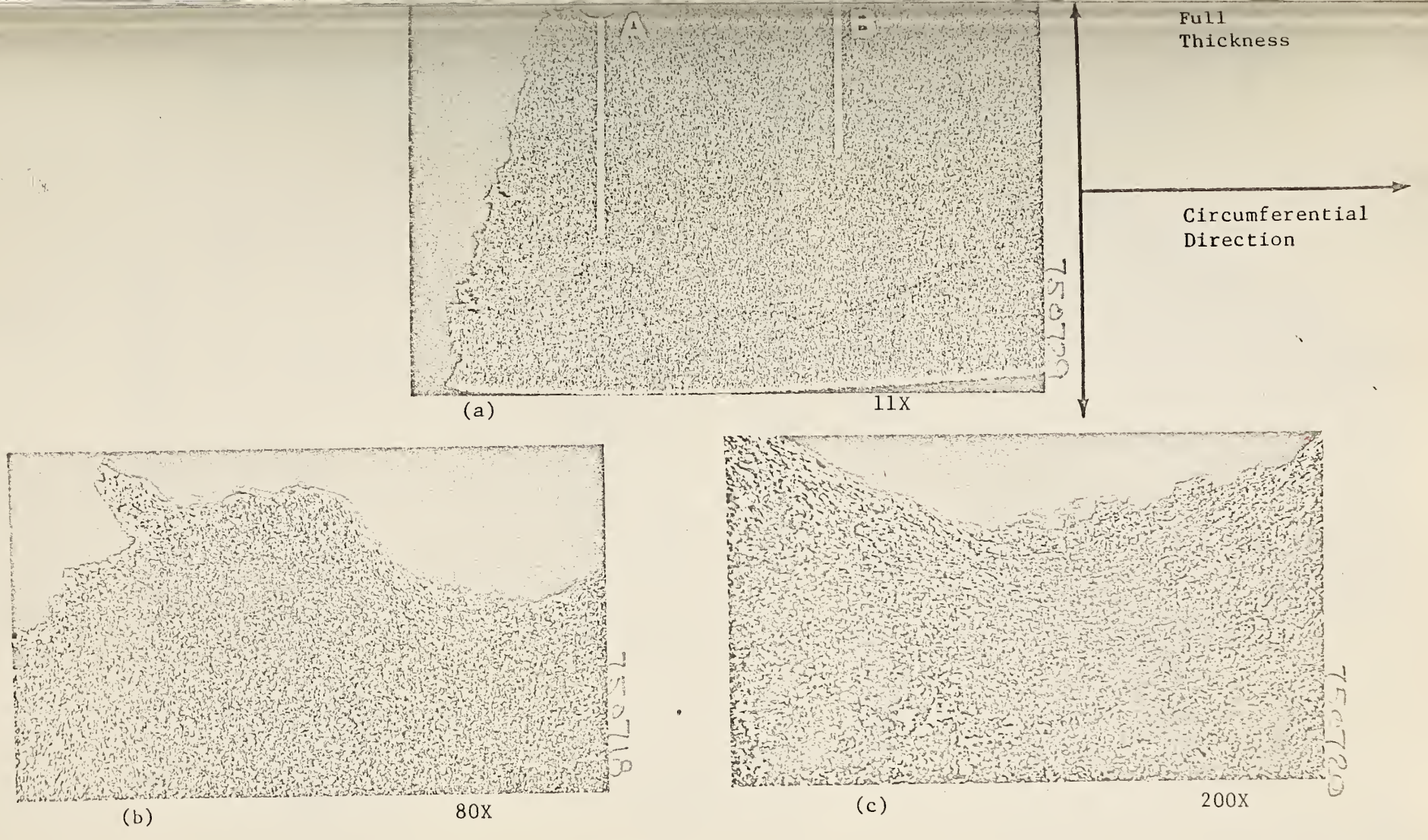

Figure 8. Fracture profile at region labeled IV in Figure 7. (a) Gouge in outside wall at fracture profile. (b) and (c) Evidence of flowed metal beneath gouge. Lines in Figure (a) show approximate paths for microhardness measurements reported in section 5.3.

Figure 9. Fracture profile of Specimen II in Figure 7, showing a gouge with a crack in the bottom.
X 80

Figure 10. Rusted regions on the external surface near the fracture origin.

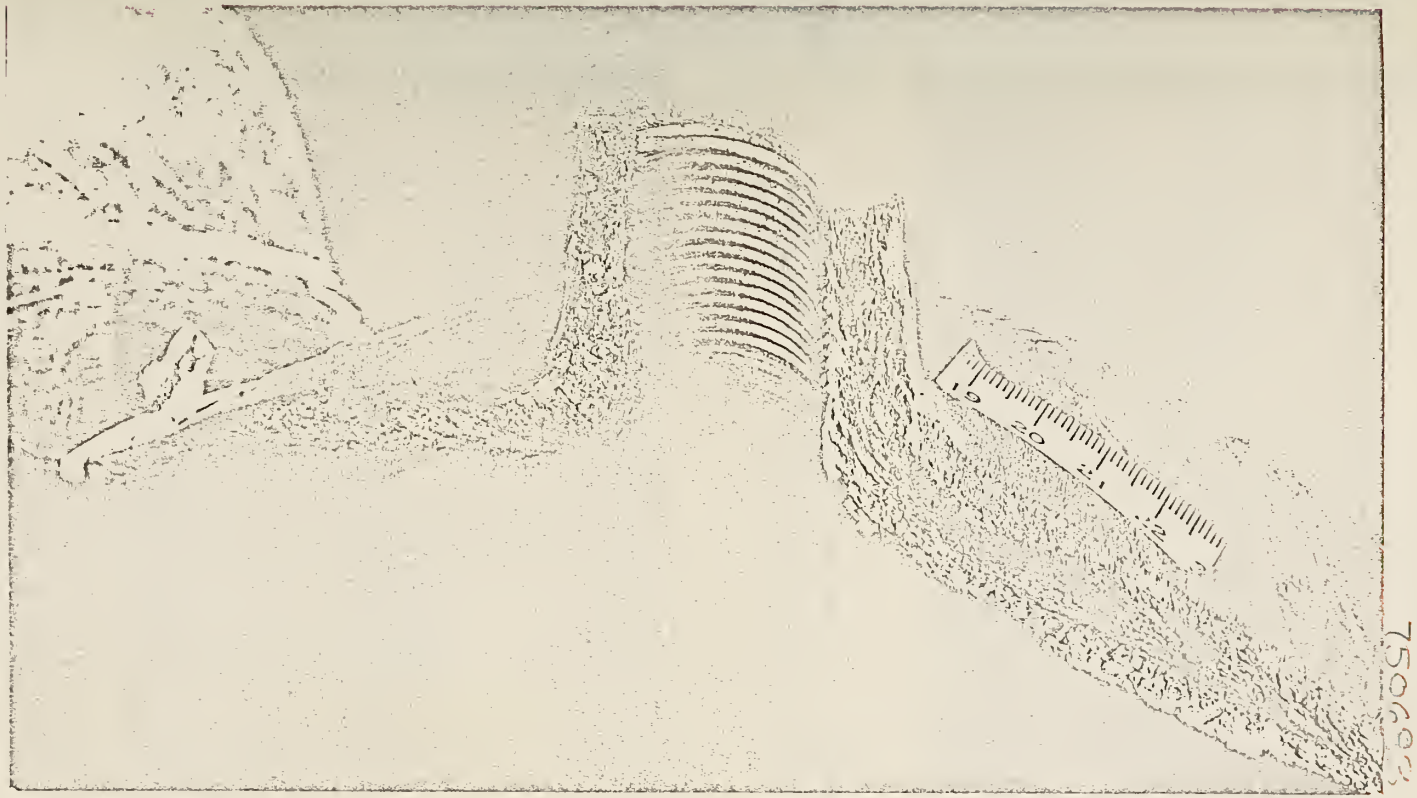

Figure 11. Fracture surface near neck of cylinder, showing fibrous fracture and relatively undamaged threads. X 1

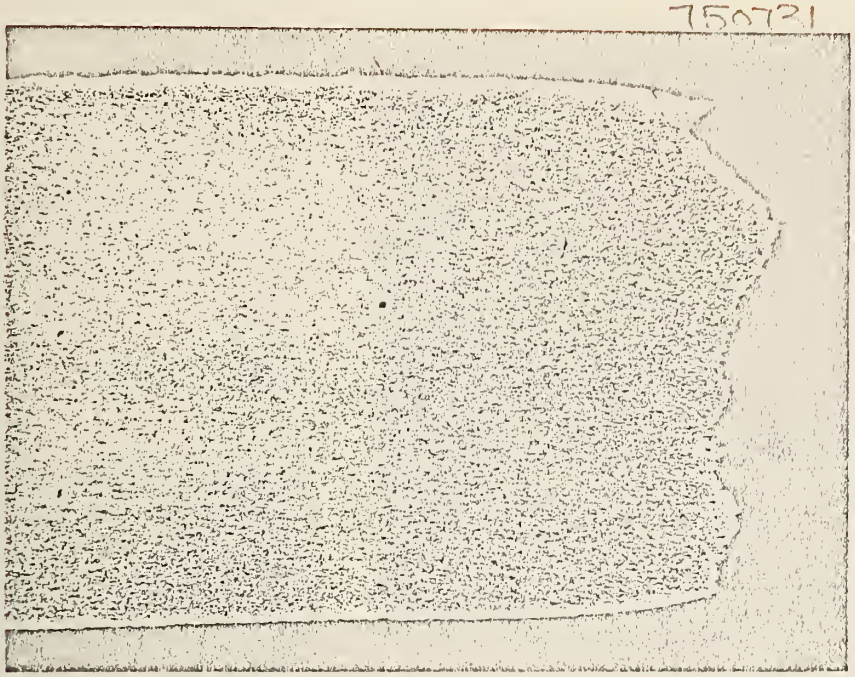

Figure 12. Fracture profile of Specimen I in Figure 7 showing wall thinning near the fracture surface. X 10

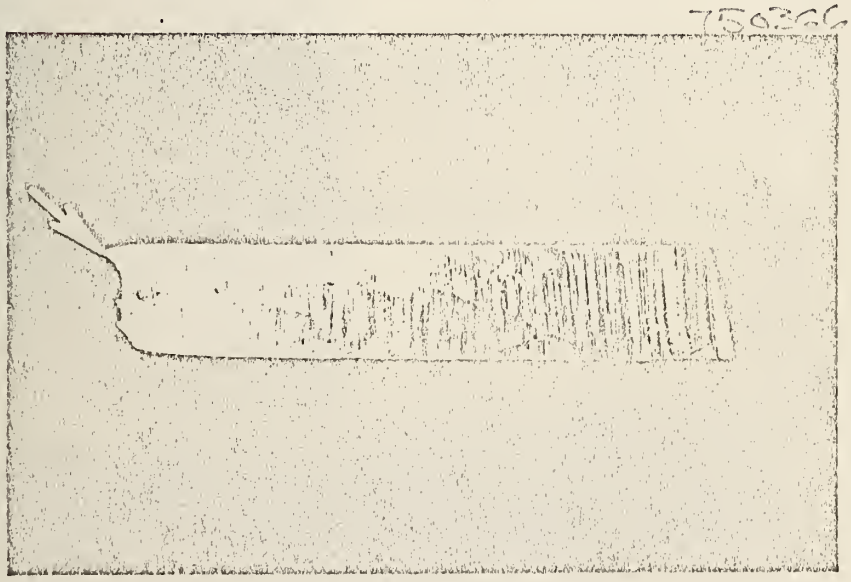

Figure 13. Cross-section through wall in region of fast-running crack, showing shear lip.

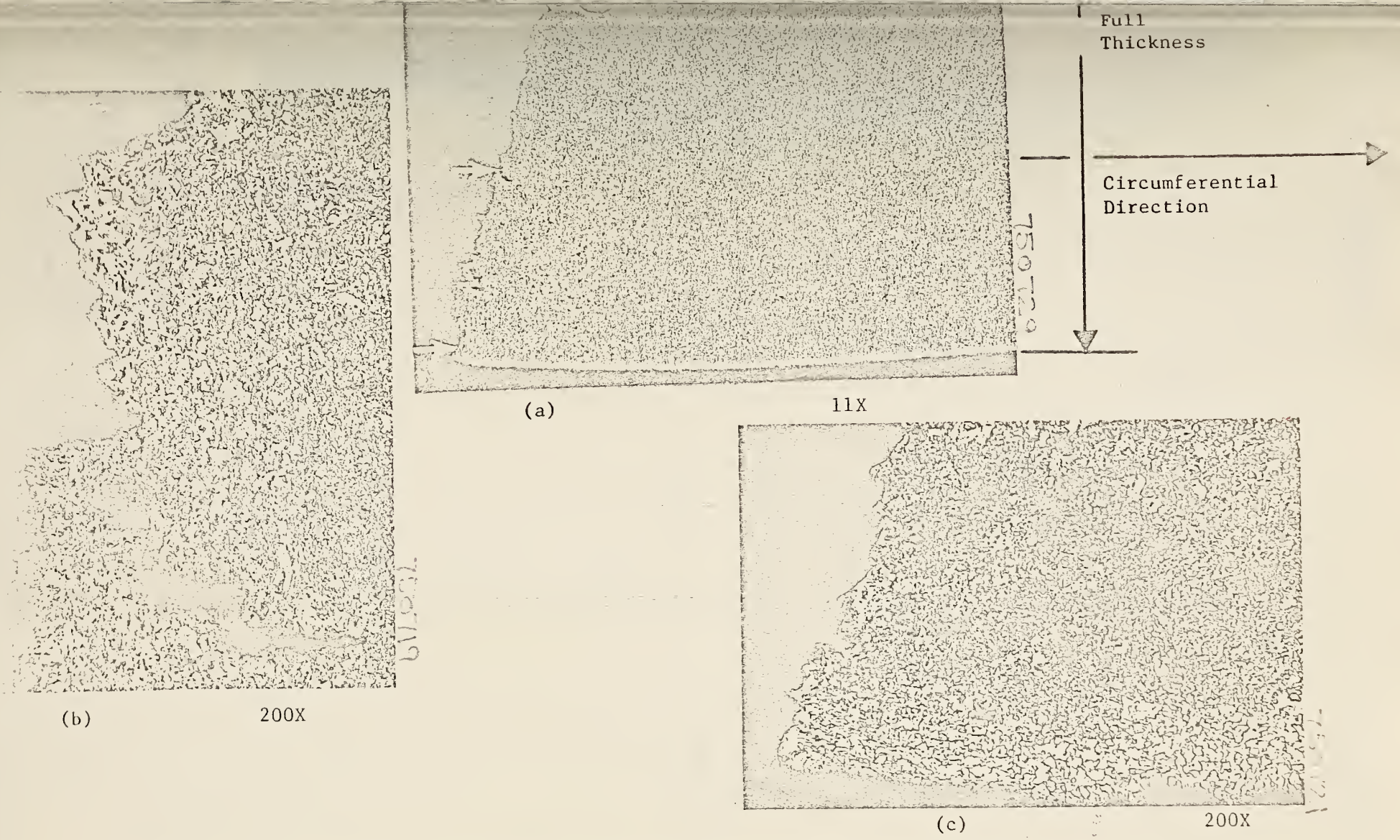

Figure 14. Fracture profile of Specimen IV in Figure 7. (a) Full-thickness profile. (b) Corrosion product and rounded recesses in rusty and discolored region of fracture origin. (c) Sharp recesses and pointed dimples in the bright region along the inside wall below the fracture origin.

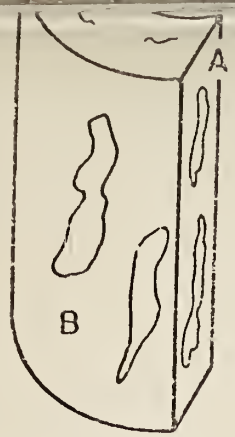

A- Longitudinal Section- Circumferential Direction

B- Longitudinal Section- Radial Direction

(a)

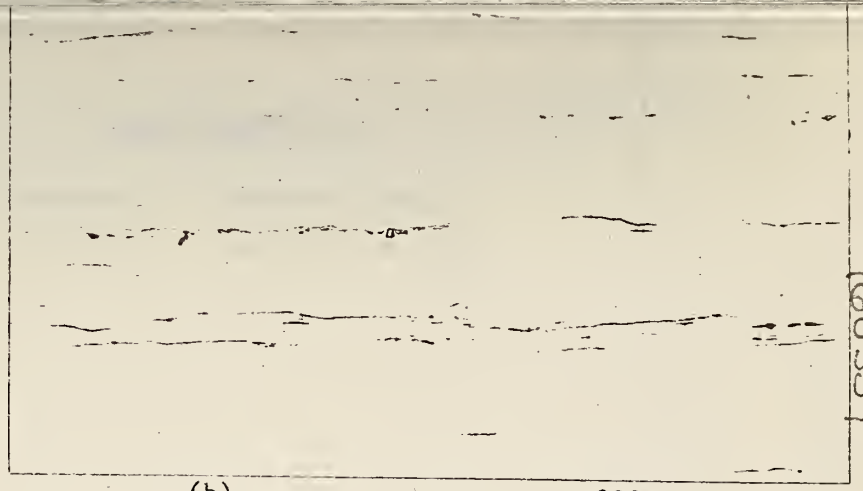

(b) 200X

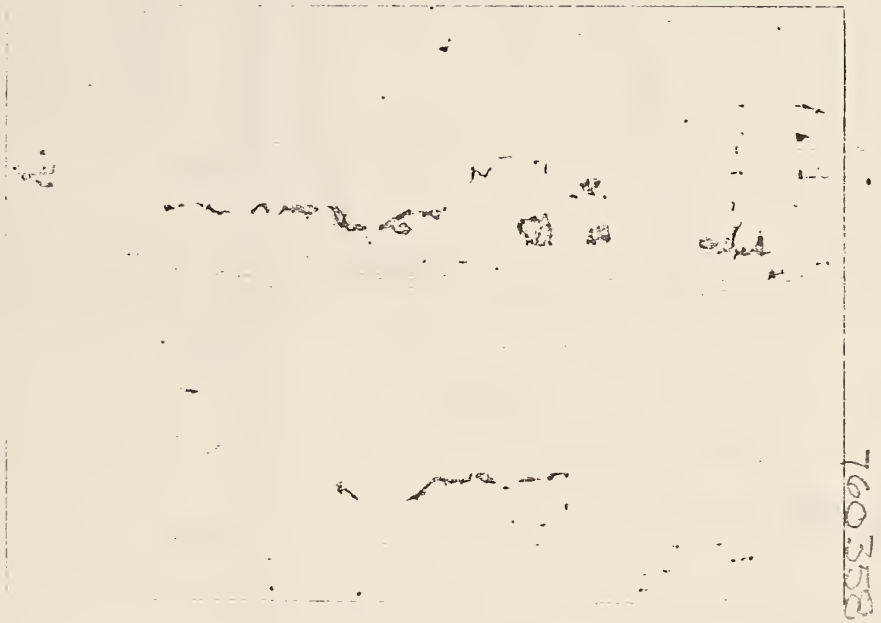

(c) 200X

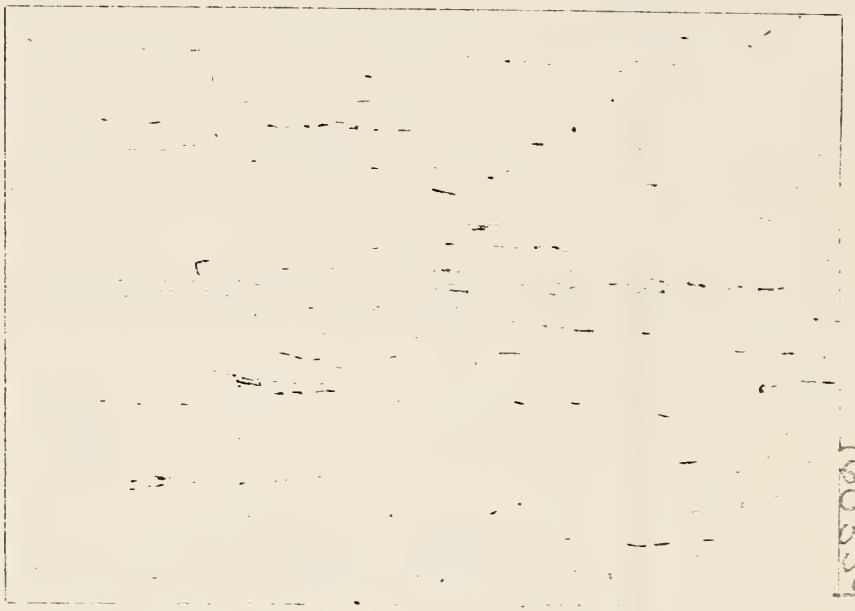

(d) 200X

Figure 15. Inclusions (a) Schematic representation and nomenclature (b) Inclusions as seen on Face A in Figure 15a. (c) Inclusions as seen on Face B in Figure 15a. (d) Inclusions as seen on Face C in Figure 15a.

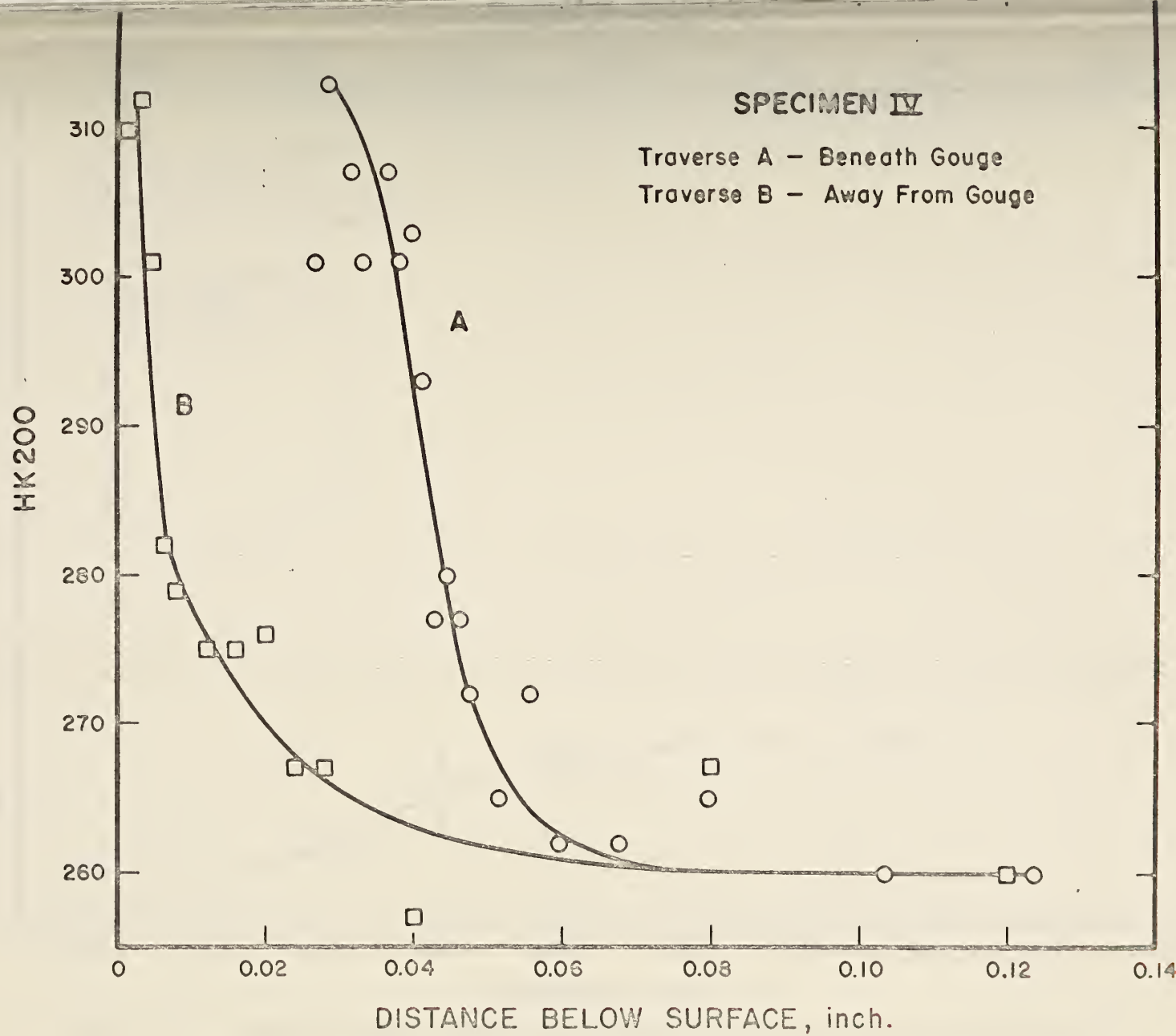

Figure 16. Knoop hardness vs. distance below surface for the fracture profile of Specimen IV in Figure 7.

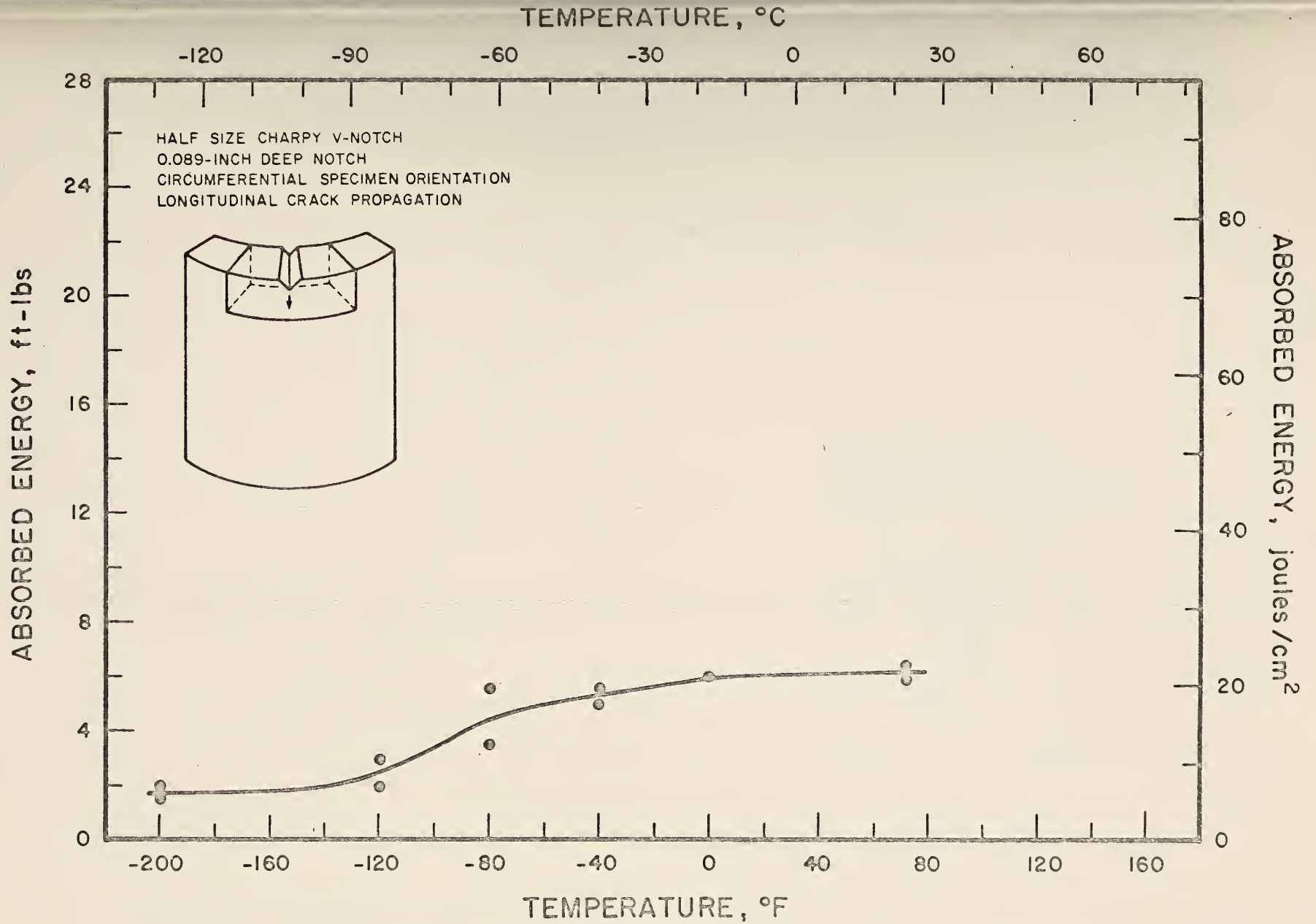

Figure 17a. Absorbed energy versus temperature for longitudinal crack propagation.

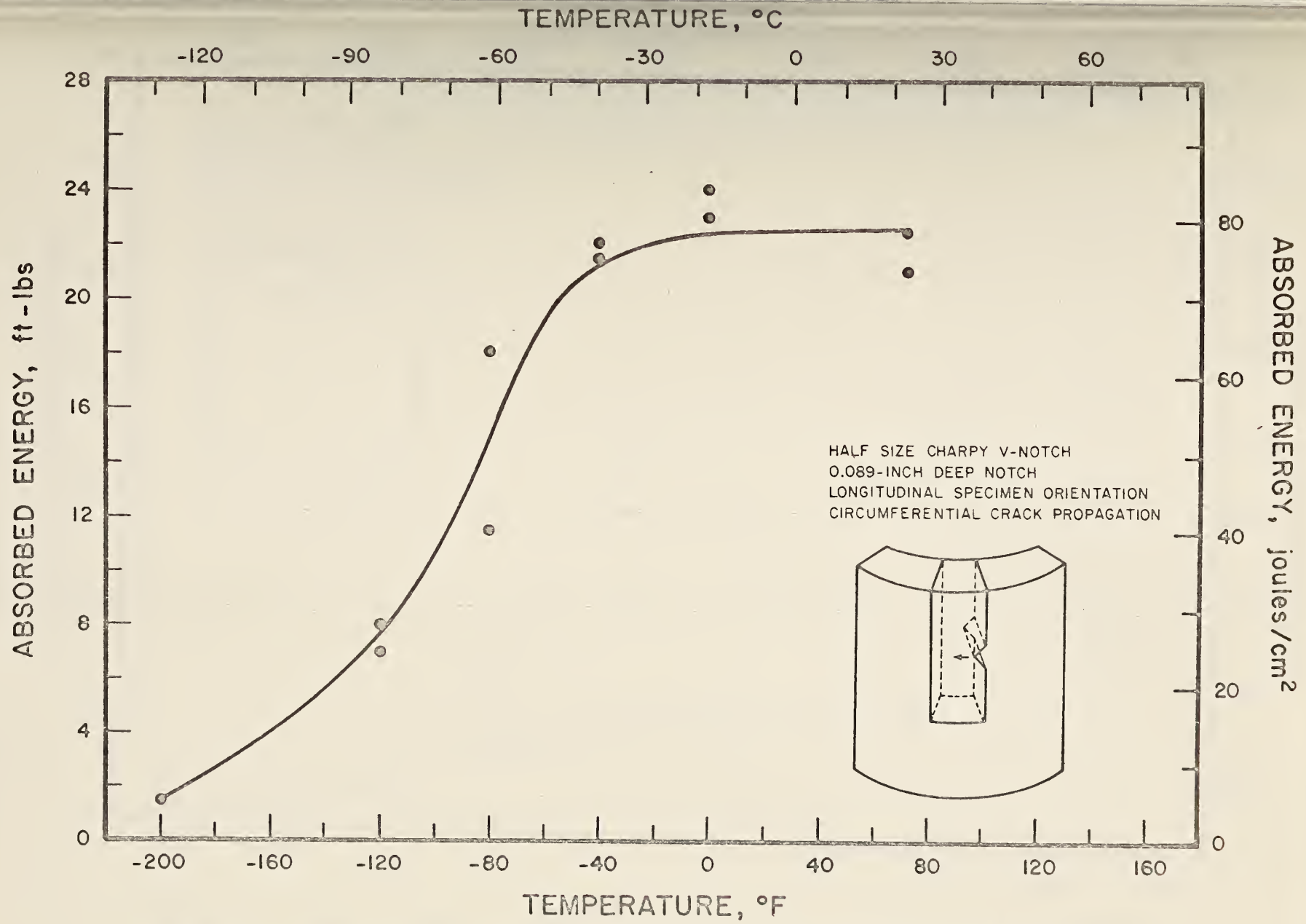

Figure 17b. Absorbed energy versus temperature for circumferential crack propagation.

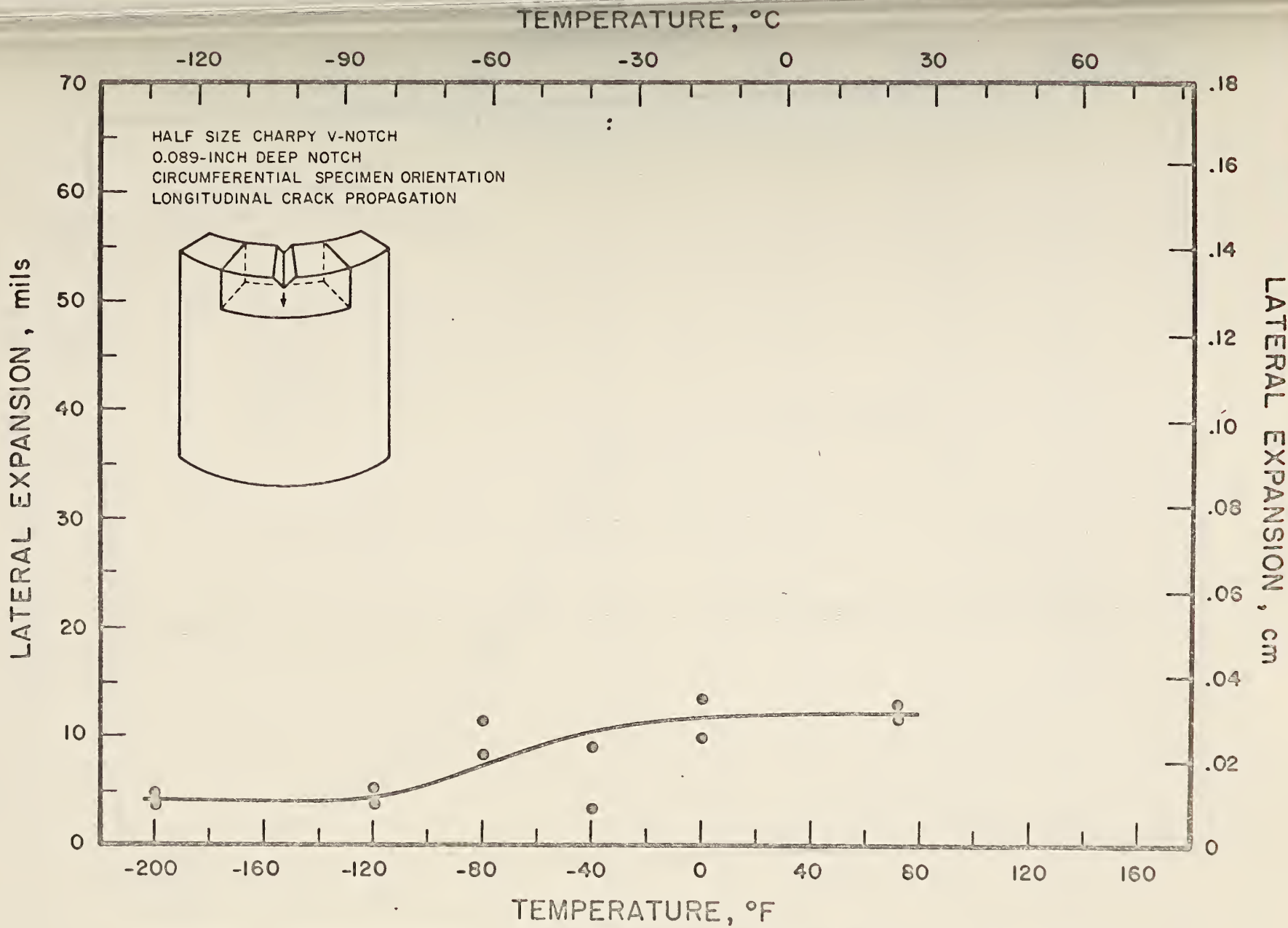

Figure 18a. Lateral expansion versus temperature for longitudinal crack propagation.

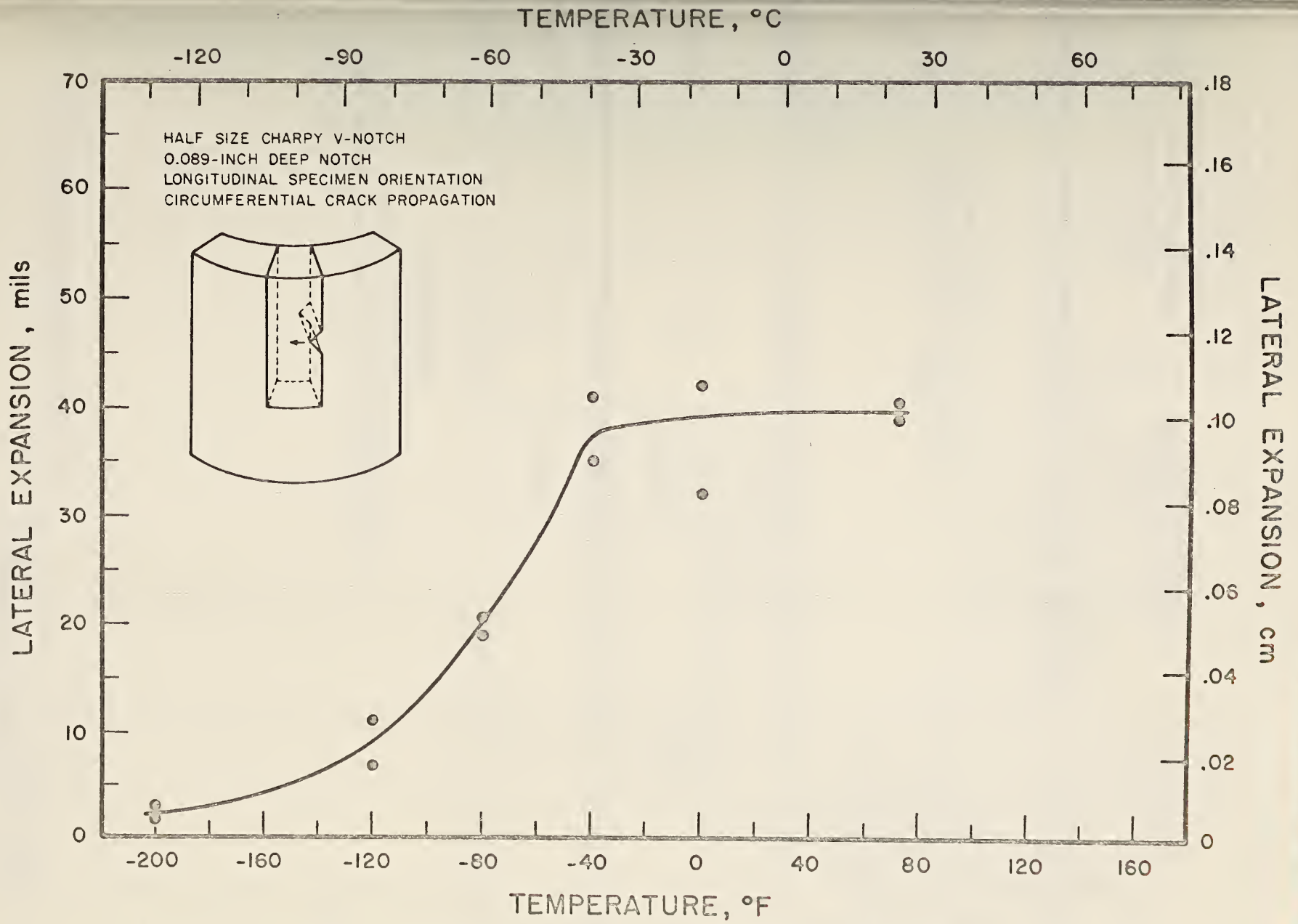

Figure 18b. Lateral expansion versus temperature for circumferential crack propagation.

U. S. DEPARTMENT OF COMMERCE
NATIONAL BUREAU OF STANDARDS
PROCUREMENT SECTION
WASHINGTON, D. C. 20234

1. [X] PURCHASE ORDER* [ ] DELIVERY ORDER
DATE ISSUED
January 26, 1978 (FY78)

2 ORDER NO
711453-1

3 SHIPPING ADDRESS
NATIONAL BUREAU OF STANDARDS
BLDG 301
711453-1
(VIA COMMERCIAL CARRIER)
Route 270 and Quince Orchard Rd
Gaithersburg, Maryland 20760
(VIA U.S MAIL)
WASHINGTON, D C 20234

PLEASE ADDRESS SHIPMENT AS SHOWN IN THIS BLOCK

SUPPLIERS ADDRESS

Pergamon Press
Maxwell House, Fairview Park
Elmsford, N.Y. 10523

Telephone.

5 SUBMIT INVOICE IN DUPLICATE SHOWING ORDER NUMBER TO
NATIONAL BUREAU OF STANDARDS
ACCOUNTING DIVISION
WASHINGTON, D. C 20234

NBS USE ONLY

COST CENTER(S)	7 OBJECT CLASS	8. I certify that the cost of this purchase is properly chargeable against the Cost Center indicated (SIGNATURE OF AUTHORIZED APPROVING OFFICER)	Date
3120211	30.1	9 REQ. NO 312-1086 / 10 DIV/SEC 312.01 / 11 WORK ORDER	
		12. Dr. R. de Wit B-120 Bldg. 223	

INVITATION NO.	14. DATE OF BID	15 F.O.B POINT	16 SHIP VIA
CONTRACT NO.	18. CODE 2B2	19. DELIVERY TIME / 20 DISCOUNT	

EM NO	22 ARTICLES OR SERVICES	23 QUANTITY	24 UNIT	25 UNIT PRICE	26 AMOUNT
	CANCELLATION Refer to purchase order 711453 dated 6/15/77 and cancel the order in its entirety due to non-delivery.				-$16.50

* Subject to attached Terms and Conditions of Purchase Order

28. JG
UNITED STATES OF AMERICA

29 TOTAL $

By Jeannette Ulaas
(Signature) CONTRACTING/ORDERING OFFICER

301-921-3257